Review

Yanan Yue[a], Jingchao Zhang[a], Xiaoduan Tang, Shen Xu and Xinwei Wang*

Thermal transport across atomic-layer material interfaces

Abstract: Emergence of two-dimensional (2D) materials with atomic-layer structures, such as graphene and MoS_2, which have excellent physical properties, provides the opportunity of substituting silicon-based micro/nanoelectronics. An important issue before large-scale applications is the heat dissipation performance of these materials, especially when they are supported on a substrate, as in most scenarios. Thermal transport across the atomic-layer interface is essential to the heat dissipation of 2D materials due to the extremely large contact area with the substrate, when compared with their atomic-scale cross-sections. Therefore, the understanding of the interfacial thermal transport is important, but the characterization is very challenging due to the limitations for temperature/thermal probing of these atomic-layer structures. In this review, widely used characterization techniques for experimental characterization as well as their results are presented. Emphasis is placed on the Raman-based technology for nm and sub-nm temperature differential characterization. Then, we present physical understanding through theoretical analysis and molecular dynamics. A few representative works about the molecular dynamics studies, including our studies on the size effect and rectification phenomenon of the graphene-Si interfaces are presented. Challenges as well as opportunities in the thermal transport study of atomic-layer structures are discussed. Though many works have been reported, there is still much room in both the development of experimental techniques as well as atomic-scale simulations for a clearer understanding of the physical fundamentals of thermal transport across the atomic-layer interfaces, considering the remarkable complexity of physical/chemical conditions at the interface.

Keywords: 2D atomic-layer; graphene; interface; Raman spectroscopy; thermal resistance.

DOI 10.1515/ntrev-2014-0024
Received September 2, 2014; accepted December 5, 2014

1 Introduction

Graphene continues receiving extensive attention due to its unique properties [1–7]. It has been experimentally validated that suspended graphene possesses an extremely high thermal conductivity, above 1000 W/m·K [7–10]. Numerical simulations and theoretical analysis have been conducted to understand the unique thermal properties of suspended graphene under various conditions [11–16]. The development of graphene synthesis methods, including physical peeling [5], chemical vapor deposition (CVD) [17], and high-temperature annealing on SiC [18], has enabled implementation of graphene flakes into micro/nanodevices [19]. Owing to its superthin thickness, graphene needs to be supported on a substrate for easier manipulation in most applications [20]. Meanwhile, the heat dissipation in graphene flakes during device operation follows two paths: one along the lateral direction of graphene layer and one in the out-of-plane direction through the interface. Although graphene's in-plane thermal conductivity is superhigh, the overall thermal conductance is relatively low, and heat dissipation of graphene in the lateral direction is greatly limited compared with the interfacial thermal transport [21]. In the thermal design of graphene-based micro/nanoelectronics, these two transport paths need to be carefully examined and thoroughly considered for better integrated thermal performance [21]. Compared with a large amount of the work measuring the thermal conductivity of suspended

[a]These authors contributed equally to this article.
***Corresponding author: Xinwei Wang,** Department of Mechanical Engineering, Iowa State University, Ames, IA 50010, USA, e-mail: xwang3@iastate.edu
Yanan Yue: School of Power and Mechanical Engineering, Wuhan University, Wuhan, Hubei 430072, China
Jingchao Zhang: Holland Computing Center, University of Nebraska, Lincoln, NE 68588, USA
Xiaoduan Tang: Department of Engineering, Thrustmaster of Texas, Inc., Houston, TX 77065, USA
Shen Xu: Department of Mechanical Engineering, Iowa State University, Ames, IA 50010, USA

graphene, not as much attention has been paid to the interfacial thermal transport between graphene or other atomic-layer materials and the substrate. This knowledge is important and needs to be clearly understood for using graphene and other 2D materials. In this review, we will summarize state-of-the-art studies about the thermal transport across atomic-layer interfaces. Thermal transport across graphene interfaces is our main focus. Studies of other novel 2D materials, like MoS_2, hexagonal boron nitride (h-BN), and silicene will also be briefly reviewed.

Thermal transport across atomic-layer interfaces is a complicated issue due to the limitation in spatial dimension and uncertainty in interfacial interactions between adjacent materials. The atomic-thin structure of graphene flakes makes it difficult to characterize interfacial thermal transport. Moreover, the structural change in preparation and transfer processes of large-scale graphene flakes makes the interface situation even more complicated [22, 23]. SiC annealing is an effective way to fabricate monolayer graphene with controllable conditions [24]. However, the extreme conditions required in the synthesis process are a big challenge to overcome. In addition, different thermal expansions of adjacent materials during the annealing process might introduce corrugations and wrinkles [25]. In other methods, like in chemical vapor deposition (CVD), quite a lot of functional groups exist at the graphene surface and are difficult to clean out [23]. During the graphene transfer process, the graphene flakes easily warp on the substrate due to their softness. Therefore, it is very common to find corrugations/wrinkles at graphene-substrate interfaces [26]. Despite the complexity of various physical/chemical conditions, the atomic bond between graphene and substrate also impacts its interfacial thermal transport [27]. The covalent bond (can be obtained from the SiC annealing method) features a tight contact and is supposed to promote energy coupling between graphene and substrate. Van der Waals bond forms a relatively loose interface and might not be good for interfacial thermal transport.

The characterization of thermal transport across a graphene interface is very challenging due to the limitation of instruments and the measurement pathways as extremely high spatial resolution for thermal probing is required. For example, if the interfacial thermal resistance is in the order of 10^{-9} K·m^2/W for a tight contact, the time constant for graphene to reach steady state (upon sudden heating) is estimated to be in the order of 10^{-13} s. This is beyond the capacity of many traditional thermal characterization methods, such as the laser flash method and traditional laser reflectance method based on nanosecond lasers. An alternative is to use the ultrafast technique by employing femtosecond lasers (pump-probe). For pump probes, the surface reflectance, in fact, gives temperature information of both graphene and substrate, which is difficult to be distinguished. Another material must be coated on top of graphene to make a more defined temperature measurement. Besides optical methods, electrical methods are also employed, for example, the 3ω method, to characterize interfacial thermal conductance [28]. The interfacial thermal transport across graphene interfaces can be understood by conducting either theoretical analysis or molecular dynamics simulations, which are effective tools to explore the energy dissipation at the atomic scale. In this review, we will summarize typical methods employed in the thermal characterizations across atomic-layer interfaces, followed by discussions about some results under various experimental or sample conditions and the physics behind them. The followed sections focus on the molecular dynamics study including models, methods, and results for the interfacial thermal transport. Finally, current challenges and opportunities in the atomic-layer thermal transport study are presented to our best knowledge.

2 Technologies for characterizing thermal transport across 2D atomic-layer interfaces

An interesting topic in the field of microscale heat transfer since late last century has been the difference in the thermophysical properties of a thin film as the thickness of the specimen shrinks to submicron scale [29]. As the sample dimension is reduced, some traditional characterization methods, which are well applied on bulk materials, might not be applicable. In the past two decades, significant progress has been made on the development of new techniques, which have been successfully applied on the measurement of thermal conductivity of thin film ranging from tens of nanometers to microns. These techniques can be classified as steady-state methods, including a microbridge method developed by Zhang and Grigoropoulos [30], thermal comparator technique [31], bolometer's method [32], and some transient methods, including the well-known 3ω method [33], thermoreflectance (photothermal) method [34], photoacoustic method [35, 36], and laser flash method [37], etc. A comprehensive review by Mirmira and Fletcher presents the measurement principles as well as results of these aforementioned techniques [29]. Not many works have been reported for measuring

the interface thermal conductance of thin films compared with above techniques for directly measuring intrinsic thermal properties. This is because of the difficulty in distinguishing interfacial thermal transport and thermal transport inside the materials of such thin thickness. One work measuring the thermal contact resistance by depositing a metal strip on dielectric substrate was conducted by Swartz and Pohl [38]. Other works either based on optical/laser methods or electrical methods have been developed from traditional characterization methods for the measurement of thin films, such as ultrafast pump probe and differential 3ω method, and so on.

When it comes to the interfacial thermal resistance between atomic-layer materials, which is an extreme case of the thin film-substrate system, great challenges for thermal characterization are brought up due to the reduction in the sample thickness. First, the sample with an atomic-thin thickness features an extremely fast heat dissipation process. Because of this reason, traditional electrical methods such as the 3ω method cannot fulfill this requirement for outranging the capacity of the instrumentation. For optical measurements, such as ultrafast pump-probe method, the surface temperature of the sample is difficult to define because large amounts of the laser will be transmitted through the material (graphene as an example). Therefore, the outlet for solving this problem can be divided as two different ways. One way is to make some modifications on the sample surface based on existent methods to either extend the characteristic time of interfacial thermal transport or make the surface temperature of the sample be well defined. The other approach is to develop new methodologies to directly distinguish surface temperature of the sample from that of the substrate without any treatment even at such small space. In this section, we will review existent works which have successfully characterized the interfacial thermal conductance of graphene interfaces based on this proposal.

2.1 3ω method for characterizing atomic-layer thermal contact resistance

The first experimental work reporting thermal contact resistance between graphene and SiO_2 employed 3ω method [28]. The principle of 3ω measurement is straightforward: a metallic wire is deposited on the sample surface serving as a heating source as well as the temperature probe. The surface needs to be polished and have excellent contact with the wire. An AC current with a frequency of ω is applied to the wire, then the heat flux and corresponding temperature oscillation will have a frequency of 2ω, which gives a change of the electrical resistance of the wire at frequency 2ω. The electrical resistance with 2ω frequency multiplied by the AC current of ω frequency gives sample's voltage variation of 3ω frequency. Therefore, the sample's thermal response to the AC heating is related to the thermal conductivity of the material and can be obtained by measuring the voltage oscillation [39]. The 3ω method has great capability of measuring semi-infinite materials as the thermal penetration length can be made larger than the heater line width, and relatively low frequencies are needed. However, if the thermal penetration depth is low, for example, in the order of nanometers (the thickness of graphene), extremely high modulation frequencies are needed. In addition, the 3ω method usually requires the line width much smaller than the thickness of the to-be-measured material to apply a sound physical model. When it comes to the application of measuring graphene structures with atomic thickness, the fabrication of such thin line heaters becomes impossible.

Targeting this challenge, Borca-Tasciuc et al. proposed a differential method of the 3ω technique. Its principle is to perform a controlled condition experiment and count the difference in the temperature rise between a film-substrate system and a same substrate system but without the film [39]. Chen et al. applied this method on the thermal contact resistance measurement between graphene and SiO_2 with a sandwiched interface [28]. Figure 1 shows the details for the microfabrication of

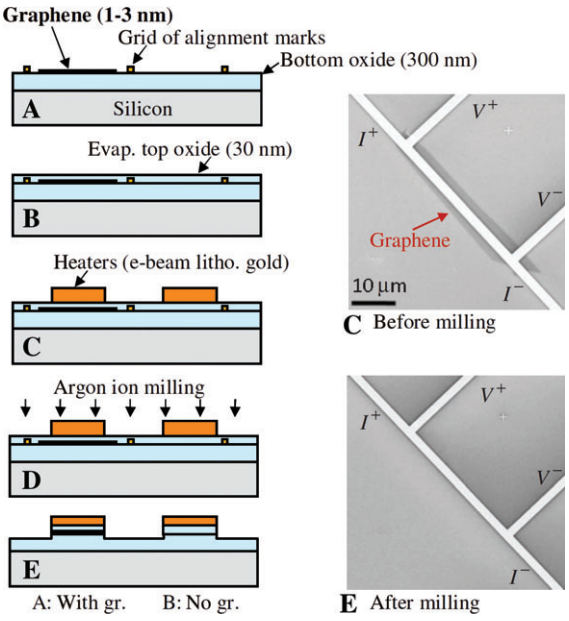

Figure 1: The sample fabrication process for the differential 3ω technique to measure the sandwiched structure of graphene-SiO_2 interface. Reproduced with permission from Reference [28]. AIP Publishing LLC, Copyright (2009).

this sandwiched structure. They first mark the positions of graphene flakes that are deposited on a silicon wafer and evaporate another oxide layer on the graphene flakes. On the oxide layer, they patterned two heaters for the 3ω technique with one on top of graphene layer and another one on top of no graphene. After this step, they used argon ion milling to trim the interface structure, ensuring one-dimensional (1D) heat conduction through the interface. During the measurement, the temperature rise for two heaters were recorded: one is for the sample measurement and the other one is used as a reference. The difference in temperature responses results from the two thermal resistances of graphene-SiO_2 interfaces (bottom and top) by assuming that the contact resistance between oxide layers (in the controlled condition) is negligible [28]. This sandwiched structure advances thermal characterization of graphene interfaces by overcoming the challenge that demands very high modulation frequencies and thin thickness of metallic wire due to the ultrathin thickness of graphene.

2.2 Pump-probe method to characterize interfacial thermal resistance

The pump-probe technique is an optical thermal characterization method that has been used extensively for thermal characterization of micro/nanofilms [40]. The principle is to use a pump (pulsed) laser to introduce laser heating. After that, the surface temperature of the sample experiences a fast rise due to the laser absorption and a slow drop due to the heat dissipation down to the substrate. A probe laser is adopted to measure surface temperature simultaneously during/after the heating by probing the reflectance of laser beam, which is temperature dependent. As the heating time is extremely short, it is desirable to use the same pulse (with much less energy) to monitor the temperature evolution after heating. This can be controlled by using a moving stage to adjust the optical path to vary the time delay. As mentioned in the introduction, the characteristic time for heat conduction across the graphene interface is extremely small due to the thin thickness. The following is a detailed physical explanation. The time constant of graphene to reach steady state can be estimated as $\rho Vc/hA$, where ρ is the density of graphene, V is its volume, A is the surface area, c is its specific heat, and h is the effective heat convection coefficient (=the inverse of interfacial thermal resistance). Taking the heat capacity of graphite for graphene (high accuracy estimation), and using interfacial thermal resistance in the order of 10^{-9} K m^2/W for a tight contact interface, the characteristic time is in the order of 10^{-13} s (100 fs). This requires the pulse duration of the laser to be at the same time scale or shorter in order to track the ultrafast temperature evolution of graphene. That is why the ultrafast technique is needed in the pump-probe method for thermal characterization of graphene interfaces.

In the measurement, the graphene layer is always coated with a metallic layer. There are two purposes for this arrangement. First, bare graphene has an extremely short time for heat dissipation as discussed above. This places great difficulties in the pump-probe technique even when a fs laser is used. By coating a metallic layer on the graphene surface, the effective thermal mass under detection is increased hundreds of times. The requirement for extremely fast temperature probing is relaxed significantly. Second, graphene has a good optical transmission (2.3% of laser absorption for a single layer at 532 nm [41], this absorptivity might vary a little bit for different wavelengths [42]). If no metallic layer is coated, most of the probing laser passes through the graphene layer to reach the substrate. As the reflected light mostly comes from the substrate rather than graphene, the measured temperature is not solely for graphene. In fact, it carries combined temperature information about both graphene and substrate surface. Therefore, it is almost impossible to characterize the interfacial thermal resistance. The coating of a metallic layer can ensure that all probed light comes from the same depth, and the temperature difference across the interface is sensible. However, the thermal transport across the metallic layer might interfere with the thermal transport across the graphene-substrate interface. The characterization result for the graphene-substrate interface might be different from the bare sample without metal coating. This effect will be discussed in detail in the next section. The principle of Zhang et al.'s pump-probe measurement is similar to the differential 3ω method: two measurement points were selected (as shown in Figure 2) with one having graphene layer insertion while the other point not [22]. The difference in temperature measurement stems from the thermal resistance of graphene interfaces. There are other works reporting the interfacial thermal resistance of graphene interfaces by using the pump-probe method [23, 43].

2.3 Raman-based thermal probing technique for interfacial thermal characterization

In recent years, a steady-state optical method, Raman thermometry, has been widely used in thermal characterization of many nanostructured materials, such as carbon

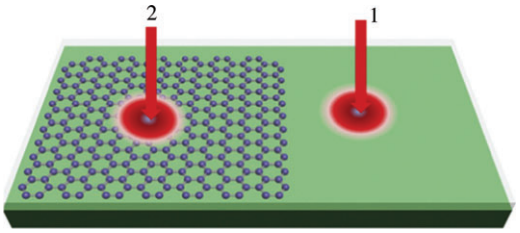

Figure 2: The principle of measuring thermal resistance of sandwiched structure of Al/graphene/Si interface by using ultrafast pump-probe method. Reproduced with permission from Reference [23]. Elsevier, Copyright (2013).

nanotube [44] and graphene [7]. In Raman thermometry, different characteristics of Raman signals excited from different materials can be used for temperature measurement. First, the peak shift (frequency or called wavenumber) is a good temperature indicator. For example, the Raman peak of graphene (G-band) shifts to the lower wavenumber direction linearly with increasing temperature at a coefficient of ~0.016 cm^{-1}/K [45]. The peak intensity is another feature for temperature probing. But it is always affected by focal levels of the optical path. Besides peak shift and intensity, Raman linewidth is the third feature for temperature probing with advantages of not being affected by thermal stresses [21]. It gives an idea of measuring thermal stress effect during Raman probing by combining the analysis of Raman frequency and peak width [25]. By using Raman thermometry, the interfacial thermal resistance can also be characterized specifically in two different pathways. Note Raman characterization is especially good at measuring the thermal transport across an ultrathin film/substrate interface as the Raman excitation laser can penetrate the film to reach the substrate and gives simultaneous temperature information about the substrate and film, thereby probing the temperature differential in space.

2.3.1 Electrical heating and Raman probing

The electrical heating method uses a constant current to induce steady-state Joule heating (as shown in Figure 3) in graphene. The heat in graphene dissipates through the interface to the substrate and induces a temperature difference across the interface. The temperature difference across the graphene interface only depends on the heating density and the interfacial resistance. As a monolayer graphene absorbs 2.3% and reflects <0.1% of the laser energy, most of the laser can penetrate graphene and reach the substrate [41]. Graphene has a good Raman scattering response, excited by only 2.3% of laser

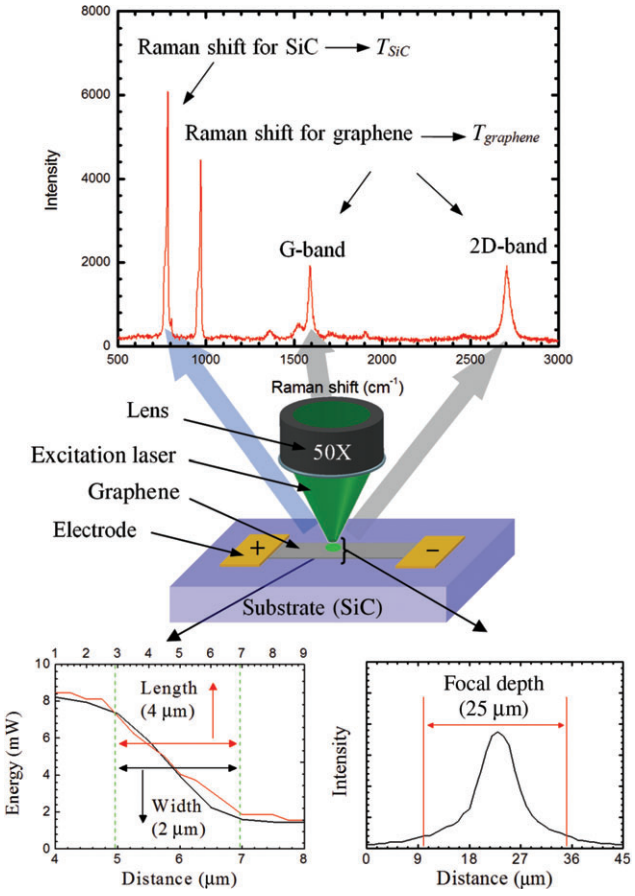

Figure 3: The schematic of electrical heating Raman-probing method to measure interfacial thermal contact resistance between graphene and 4H-SiC. Reproduced with permission from Reference [21]. John Wiley and Sons, Copyright (2011).

energy. If the substrate is a good Raman-sensible material, too (for example, silicon wafer), the scattered Raman signal contains temperature information about both graphene and silicon. This appears on one Raman spectrum as two distinctive Raman peaks. From these peaks, the temperature of adjacent materials can be extracted and used for thermal resistance evaluation [21]. The Joule heating method features a uniform and very controllable heating density, which can be easily manipulated for different experimental conditions. However, Joule heating requires the fabrication of an electric circuit. Also, the laser heating involved in Raman probing is a problem and needs to be carefully considered during temperature calibration. In addition, the thermal stress during Joule heating is another issue, which needs more attention, especially for high temperature measurement. Yue et al. conducted the measurement of thermal resistance between epitaxial graphene and 4H-SiC by using the electrical heating and Raman probing method [21]. As shown in Figure 3, a trilayer graphene is connected with a current

source that supplies steady-state Joule heating. A probing laser is focused on the graphene layer for Raman excitation. The obtained Raman signal can be used to determine the temperature of both graphene and SiC. It needs to be noticed that the obtained temperature of SiC is not from the surface adjacent to graphene. It is an average value of SiC within the laser penetration depth/focal depth. This needs to be considered in the thermal resistance calculation [21]. Actually, the portion of the Raman signal from a different depth of laser penetration, which contributes to the measured temperature, is not constant. A precedent calibration experiment needs to be performed to characterize the intensity of Raman signal at different focal levels. Therefore, the surface temperature of SiC can be defined as $\overline{T}+\beta\cdot\int_0^{\Delta z/2} z\cdot I\cdot dz / \int_0^{\Delta z/2} I\cdot dz$, where $\overline{T}$ is the measured temperature of SiC from Raman signal; β is the temperature slope of SiC along the focal depth, which can be determined as q''/k (k is the thermal conductivity of SiC). A 0 point for the derivation is set at the graphene sheet whose thickness is in the order of nanometer and can be ignored comparing with the focal depth (in the order of micrometer). I is the distribution of Raman intensity obtained from the above calibration experiment.

2.3.2 Photon heating and Raman probing

Besides electrical heating, laser heating is an alternative to induce temperature difference for interfacial thermal characterization. The laser heating method can effectively overcome the challenge in micro/nanofabrication of electrical circuit, and provides great advantages in measuring samples of extremely small sizes. Also, in the Joule heating method, if the sample is not uniform, for instance, the graphene layer number distribution is not uniform in space, the Joule heating density will not be uniform in space. This could introduce considerable uncertainty in determining the heat flux across the interface in the Raman probing region. The localized heating effect in the laser heating method makes sure the laser heating region and the Raman probing region are the same. This design helps improve the measurement accuracy significantly. Compared with the thickness of graphene, the heating laser beam is much larger, and the heat conduction across the graphene interface can be regarded as 1D. Cai et al. used a probe laser from Raman spectrometer to heat graphene and used a modified thermal diffusion model for supported graphene [46]. The Bessel function used in their work involves both thermal conductivity of graphene and interfacial thermal resistance. The heating density can be adjusted by switching different focal lenses, and the interfacial thermal resistance can be estimated accordingly [46]. The work by Tang et al. used two lasers to realize this technique: the laser with a higher energy is used as the heating source of graphene and the other one with much less energy equipped with Raman spectrometer is used solely as thermometer for temperature probing [25]. As shown in Figure 4, the focal areas of the two lasers

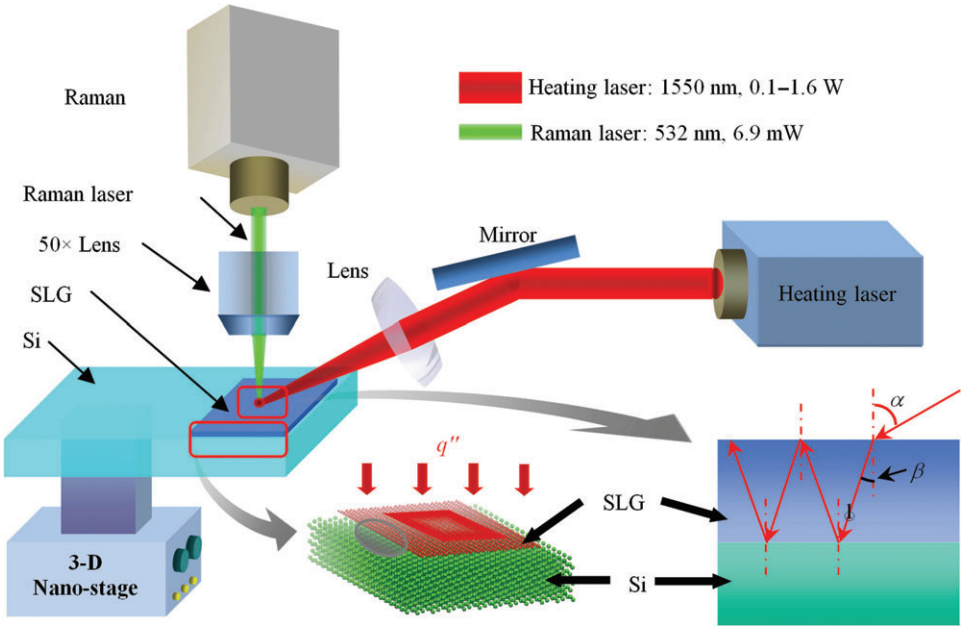

Figure 4: The schematic of photon heating Raman-probing method to measure interfacial thermal contact resistance of graphene interfaces. Reproduced with permission from Reference [25]. American Chemical Society, Copyright (2014).

are overlapped, and the probing area needs to be smaller than the heating area. This separate photon heating and Raman probing design has the great advantage to avoid any slight optical alignment shift during objective lens change in confocal Raman. Our past experience confirms that a small change in the optical alignment can introduce undesired shift in the Raman spectrum, including its wavenumber, linewidth, and intensity. In the separate photon heating and Raman probing method, the Raman system stays at the exactly same configuration, and only the power of the heating laser is varied.

In Tang et al.'s work, two different interfaces have been characterized: graphene-Si interface and graphene-SiO_2 interface [25]. For the interfacial thermal characterization between graphene and SiO_2, the heating laser is focused on the graphene layer through the substrate. The purpose of this arrangement is to make the optical path easier to adjust based on the Raman setup used in this experiment. However, this arrangement requires the substrate material to be transparent to the heating laser. Very recent work by Tang et al. also employed this technique/setup to characterize the interfacial thermal resistance between graphene and SiC [47]. In this photon-heating Raman-probing method, the laser absorption in graphene needs to be carefully evaluated as the amount of energy absorbed in graphene directly determines the value of thermal contact resistance. In Tang et al.'s work, the interfacial thermal resistance was characterized by using both Raman shift and width methods [25, 47]. The difference between these two methods was used to evaluate the thermal stress during laser heating. In addition, the Raman intensity was examined to explore optical interference effect between graphene and substrate, which validated the high thermal contact resistance induced by the corrugation of graphene [25, 47].

The separate laser heating method developed by Tang et al. makes it possible to control the heating by using a desired laser wavelength [47]. Also, the heating laser energy can be continuously adjusted without touching the sample. This guarantees the whole optical path stays exactly the same during Raman-based thermal characterization. This is extremely important for Raman thermal probing as any small change in optical alignment will shift the Raman signal (peak position, intensity, and linewidth). Caution should be exercised for using different objectives or neutral density filter to adjust the Raman excitation laser energy to vary the heating level. This extensive and careful systematic study has revealed this kind of operation will induce slight optical path change and result in undesired Raman scattering change.

3 Thermal transport across atomic-layer interface: physics and understanding

In this section, experimental results on interfacial thermal resistance measured by the methods referred in the last section are classified into two scenarios to discuss. A summary of experimental results is listed in Table 1.

3.1 Graphene interfaces within the sandwiched structure

For the 3ω and ultrafast methods, direct measurement on the bare graphene interface is not applicable as analyzed in the above section. In Chen et al.'s work, graphene flakes with different thickness from 1.2 nm to 3 nm were sandwiched between SiO_2 layers. The thermal contact resistance was measured from 5.6×10^{-9} to 1.2×10^{-8} K m^2/W with temperatures from 42 to 310 K [28]. The thermal resistance has a down trend with temperature for all samples. The measured low contact resistance might stem from the coating of a top oxide layer on the bare graphene for the differential 3ω measurement because the coating of the oxide layer could make the graphene interface be much tighter than the original state. The phonon transmission from the bare graphene layer to the substrate could be significantly different from the sandwiched graphene structure between two oxide materials. As the metallic strip acts as the heater and the temperature monitor of the measurement, the top-down phonon transmission between two oxide layers might dominate the thermal transport, and the interfacial thermal contacts with graphene layer (two sides) is not as important.

The same issue induced by the extra metallic coating also exists in the thermal characterization of graphene interfaces by using the pump-probe method [22, 23, 48]. The coated metallic layer on graphene is used for absorption of laser pulse and facilitating well-defined thermal probing. However, how the deposition of additional metallic layer affects thermal transport across the atomic-layer interface remains unclear. In Zhang et al.'s work, the embedded graphene between the thermal evaporated Al film and Si substrate can enhance interfacial thermal transport, which means there is apparently negative thermal contact resistance between graphene and interfacial materials [22]. It is explained that the graphene prevents the diffusion of Au atoms into substrate and reduces the thickness of the intermixing layer. To validate this speculation, they conducted the measurement for

Table 1: Summary of thermal contact resistance of grapheme interfaces.

Interface	Thermal resistance ($K\ m^2/W$)	Method	References
Al/Graphene/SiO_2	5.6×10^{-9} to 1.2×10^{-8}	3ω Method	[28]
Magnetron sputtered Al/Graphene/Si	1.6×10^{-8}	Pump probe	[22]
Au/Ti/Graphene/SiO_2	4×10^{-8}	Pump probe	[48]
Al/Graphene/SiO_2	$3.3–5\times10^{-8}$	Pump probe	[23]
Graphene/SiO_2	2×10^{-8}	Pump probe	[43]
Tri-layer graphene/4H-SiC	5.3×10^{-5}	Electrical heating Raman probing	[21]
Graphene/hexagonal boron nitride (h-BN)	1.32×10^{-7}	Electrical heating Raman probing	[49]
Graphene/Si	3.57×10^{-8}	Raman method	[46]
Graphene/Si	5.46×10^{-3}	Photon heating Raman probing	[25]
Graphene/SiO_2	3.76×10^{-3}	Photon heating Raman probing	[25]
Graphene/SiC	2.44×10^{-3}	Photon heating Raman probing	[47]
Graphene/6H-SiC	1×10^{-8}	Molecular dynamics	[50]
CNT/CNT	6.46×10^{-8}	Molecular dynamics	[51]
Graphene/Si	3.52×10^{-8}	Molecular dynamics	[52]
Graphene/graphene	$1.48–4.88\times10^{-11}$	Molecular dynamics	[52]
Graphene/6H-SiC	$2\times10^{-8}–1\times10^{-7}$	Molecular dynamics	[53]
Graphene/graphene	$0.2–4\times10^{-9}$	Molecular dynamics	[54]
Graphene/SiO_2	4×10^{-8}	Theoretical calculation	[55]

magnetron-sputtered Al films. It is found that the embedded graphene contributes to the interfacial thermal resistance for magnetron-sputtered Al film due to the increased number of interfaces [22]. Their results prove that different coatings on graphene layer would change the interfacial thermal transport significantly. Sometimes, the thermal contact resistance of graphene interfaces can be shadowed by the thermal transport from the coated layer to substrate. Koh et al. also conducted the pump-probe experiment to measure the overall thermal conductance of Au/Ti/graphene/SiO_2 interface as 25 MW/m^2 K, which is much smaller than that of the Au/Ti/SiO_2 interface [48]. They attribute the reduction in phonon transmission to the limit in graphene/metal contact [48]. Hopkins et al. studied the effect of functional groups on thermal conductance of graphene interface [23]. The measured values for Al/monolayer graphene/SiO_2 ranges from 20 to 30 MW/m^2 K at temperatures from 100 K to 400 K. They revealed that the hydrogen functionalization process introduces disorder in graphene and does not add any bonding mechanism. Oxygen functionalization increases the covalent bond between Al and graphene, thus, improving the thermal conductance between them [23].

For graphene/semiconductor interfaces, the main energy carrier in both graphene and substrate is phonon. Therefore, the energy transport is mainly dominated by phonon transmission. When it comes to the graphene/metal interfaces, as the electron is the main energy carrier in metals, while phonon dominates heat transport in graphene, both phonon and electron participate in the interfacial energy transport: that is, phonon/phonon interaction, electron/phonon interaction, and electron/electron interaction are all involved in the energy transmission. Koh et al. found that phonon/phonon interaction still dominates the thermal transport across graphene-metal interfaces [48]. For sandwiched graphene structures, the deposited layer of either metallic atoms or semiconductor atoms would impact the energy transport across the graphene interface. As the energy dissipates from the deposition layer to the substrate, and monolayer graphene has only atomic-level thickness, the energy transport can happen directly between the deposition layer and the substrate. The existence of the graphene interface has a minor effect during this energy transport because the atomic potential still plays an important role between deposition atoms and substrate. It is difficult to define whether the existence of the graphene layer would promote the energy transport between deposition layer and substrate or weaken it. This is why the graphene interface thermal resistance is small for sandwiched structures compared with unconstrained interfaces.

3.2 Unconstrained graphene interface

The unique property of graphene and its atomic thickness prevents the application of the aforementioned either 3ω or pump-probe method directly on virgin graphene interfaces. For unconstrained graphene interfaces, Raman thermometry is a more effective method because the

temperature difference of materials across the interface can be directly distinguished by a single shot of Raman spectrum. It provides the most direct interface characterization based on photon scattering, and the interface thermal transport is not affected by the coating treatment. Current works available based on Raman thermometry can be divided into two categories: electrical heating and laser heating. Electrical heating can generate a uniform temperature field for heat dissipation, and the physical model for interfacial thermal transport is simple. The drawback is that the applicable graphene interfaces involves much uncertainties in sample morphology (including the corrugation, breaks). The undesired heat accumulation at the breaks/corrugations might contribute large uncertainties in the determination of interfacial thermal resistance.

The measurement results under intensive Joule heating show that the interfacial thermal resistance is increased by orders of magnitude due to the interface mismatch induced by thermal expansion effect. In Yue et al.'s experiment, the thermal contact resistance between trilayer graphene and SiC is measured as 5.3×10^{-5} K m^2/W by using the electrical-heating Raman-probing method [21]. Recently, Chen et al. used the electrical-heating method to measure the interface conductance across graphene/hexagonal boron nitride heterojunction as 7.4×10^6 W/m^2 K. This value is also orders of magnitude lower than the values measured by the pump-probe method. They attributed the low thermal conductance to the high electrical power applied on the graphene layer [49]. The significance of Yue et al. and Chen et al.'s works is achieving the nanoscale spatial resolution for direct temperature probing without any coating or pretreatment [21, 49]. Actually, the thermal resistance between boron nitride and silicon substrate can also be extracted across two interfaces by this direct temperature probing method. Therefore, thermal conductance across two nanoscale interfaces can be readily obtained from a single shot of Raman spectrum.

The laser heating method is very effective for the localized heating experiment, as well as reaching a predefined level of heating easily. It avoids the circuit fabrication for Joule heating, but the optical alignment needs to be carefully adjusted to make sure the focal point of the probing laser falls inside the heating area. The thermal model is a little more complicated, but it is an effective method to study the localized heat transfer at the graphene interface. In Cai et al.'s work, the interfacial thermal conductance between graphene and Si substrate is measured as 28+16/-9.2 MW/m^2 K [46]. Tang et al. determined the thermal conductance (G_t) as 183±10 and 266±10 W/m^2 K for graphene/Si and graphene/SiO_2 interfaces, which is five orders of magnitude lower than the normal thermal interfacial conductance [25]. Recent work also by Tang et al. reported the thermal conductance (G_t) as 410±7 W/m^2 K for graphene/SiC interface [47]. Their detailed surface morphology study revealed large graphene corrugation. The extremely low thermal conductance stems from the decoupling effect of phonon transport across the graphene interface due to the loose interface mechanical coupling, which is validated by strain analysis from Raman peak shift. In their work, the Raman intensity was employed as an effective tool to study the interference effect between graphene and substrate to probe the delamination phenomenon at the interface [25, 47]. A detailed study in that work revealed that a slight increase in the interface spacing will significantly increase the interfacial thermal resistance. The Raman-based dual thermal probing method provides a pathway for comprehensive study of complex structures of graphene interfaces, especially for corrugation/wrinkling problems. In Raman-based thermal transport study, the Raman shift (wave number) is widely used to determine the temperature. It needs to be pointed out that the Raman shift can be affected by both temperature and stress. Therefore, comprehensive Raman spectrum evaluation, including Raman shift, linewidth, and Raman intensity is always needed to give the best evaluation of the temperature rise and interface thermal resistance.

As the Raman method is based on the scattering effect of the atomic material rather than on the reflection of the probing laser in the pump-probe method, it requires the to-be-measured material be transparent to let the probe laser reach the substrate to excite the Raman signal of the substrate material. The unconstrained graphene interface has a thickness of nanometers and is perfect for applying Raman thermometry. As the measurement accuracy of Raman thermometry is determined by the resolution of the spectrometer, which always has a limit, for tight interfaces, which feature a small thermal contact resistance, the temperature difference across the interface is small and is difficult to probe by the Raman method. An effective way is to increase heat flux density to increase the temperature difference. On the other hand, the high temperatures induced by the high heat flux density could result in thermal expansion mismatch. If the mismatch is strong, delamination at the tight interface could happen and will break the original tight contact. In addition, the mismatch at the interface builds up the local stress. Therefore, sole use of Raman frequency (wave number) method cannot guarantee the accuracy of temperature determination as the signal is also affected by the local strain/stress. Raman linewidth is preferred for the temperature measurement under the condition that the focal level of probing

laser during the measurement is kept constant. Therefore, the combined analysis based on Raman shift, linewidth, and intensity gives more detailed and reliable information about the thermal transport and morphology of graphene interfaces. From the other point of view, as the temperature probing resolution is limited by the resolution of spectrometer, and only large temperature differences can be probed by the Raman method, the Raman method is very effective in measuring the interface material with loose contact or with large interface thermal resistance. This conclusion is based on the steady-state measurement. For transient measurement, the temperature differential can be distinguished by applying a high-energy laser pulse, which combines the advantages of ultrafast pump-probe method and Raman thermometry. This allows one to apply the Raman method to measure graphene interfaces with tight contact. In summary, the Raman method can be used in either steady-state thermal characterization or transient measurement for measuring tight or loose interfaces. Current work is not available to date, and this proposal will be detailed in the section of future work.

4 Atomistic-scale modeling of interface thermal transport: methods

4.1 Non-equilibrium molecular dynamics

Non-equilibrium molecular dynamics (NEMD) simulation is widely used for calculations of interfacial thermal resistance. By applying a heating source and heat sink separately at the opposite edges of the composite system, a temperature gradient will be built up in the heat flux direction after the system reaches thermal equilibrium. The temperature drop occurring at the interface of the contact area can be used to determine the thermal resistance value according to this equation: $R=\Delta T\cdot A/q$, where R is the interfacial thermal resistance, ΔT is the temperature difference/drop across the interface, A is the cross-sectional area, and q is the heat flux across the interface.

For bulk materials containing tens of atomic layers in the heat flux direction, the NEMD method has been extensively used to calculate the interfacial thermal resistance [50–52, 56–58]. After thermal equilibrium calculations, the thermal conductivity of each material can be calculated by linear fitting of the temperature profile. The heating and cooling regions are excluded from this fitting process to reduce errors [51, 52, 57, 58]. In MD simulations, kinetic energies are constantly added/subtracted in the heating/cooling areas for temperature controls. In this ultrafast energy exchange process, in the heating/cooling regions, kinetic and potential energies are in non-equilibrium state, and phonon boundary scattering is furious at the interface between the heating/unheating (or cooling/uncooling) regions. Therefore, the temperature drop is nonuniform in these regions and must be excluded from thermal conductivity calculation.

For two-dimensional (2D) materials like graphene, the NEMD method for thermal contact resistance calculations should be used with great caution. Based on the above discussions, if a heat flux is directly imposed on the 2D material, the temperatures calculated from this region could be illusory, and temperature jump at the interface will be inaccurate. To avoid this controversial situation, the 2D material can be put in the middle of a sandwiched structure [50, 53, 54]. After the system reaches thermal equilibrium, the temperature of the 2D material and its adjacent layers will be recorded and used for thermal contact resistance calculations. For this modeling treatment, the materials on both sides of the 2D material could have long-range interaction and exchange energy directly without via the 2D material (if the 2D material is very thin). This will change the interface energy coupling scenario. Also, the extra material on the side of the 2D material will constrain the phonon movement of the 2D material, thereby, leading to undesired phonon alteration.

4.2 Numerical pump-probe method

As introduced in the above sections, the pump-probe method also has been employed extensively in thermal characterization of bulk materials and thin films [22, 27, 43, 59–61]. In this pump-probe technique, a high-repetition rate pulse source is favored than low-repetition rate amplified systems as high-repetition rate allows for pump-beam modulation and lock-in detection at high frequencies. However, under such high repetition rates, there is no sufficient time for the system to reach thermal equilibrium between laser pulses. The heating effects will accumulate over time. Schmidt et al. discussed the relationship between pulse accumulation and radial heat conduction in the pump-probe method and demonstrated how pulse accumulation allows for probing of two thermal length scales simultaneously [59]. A pump-probe method using molecular dynamics simulation has been used in our research to study the surface roughness effect on thermal transport across the graphene-silicon interface [62]. The principle of the pump-probe methodology

in MD simulation is the same as experimental characterization. Compared to the traditional NEMD method, this technique is focused on the dynamic thermal response of the system and can greatly reduce the computation time. Also, it eliminates the undesired phonon scattering in the 2D material due to localized heating/cooling.

4.3 Other methods

Theoretical methods using the acoustic mismatch model (AMM) [63, 64] and diffuse mismatch model (DMM) [65] are widely used to study interfacial thermal resistance properties at low temperatures. The AMM assumes that the interface between two materials is perfectly specular, and the phonons either transmitting or reflecting at the interface should obey Snell's law. However, this ideal case only represents a limited number of modern devices. To better describe the interface phonon scattering, the diffuse mismatch model is developed. The DMM assumes that when crossing the interface, the phonons will lose track of which side of the interface they come from, as well as their former directions and polarizations. The transmissivity has no angular or phonon mode dependency because of the nature of diffusive scattering. Both AMM and DMM can predict experimental data quite well at low temperatures [38, 65]. However, at high temperatures, most of the practical material systems are not consistent with the corresponding assumptions, which will cause great discrepancy in the interfacial thermal resistance between the model predictions and experimental results. Theoretical models have been developed to study the thermal transfer across weakly coupled systems with a flat interface. Thermal contact resistance between graphene and amorphous SiO_2 is calculated at 4×10^{-8} K m^2/W by estimating the heat transfer coefficient at the interface [55]. A summary of simulation and theoretical calculation results is also presented in Table 1.

5 Interface thermal transport modeling: physics and understanding

5.1 Interfacial thermal resistance determination

While the in-plane thermal transport in graphene can be sustained by acoustic vibrational modes called phonons, the dominant heat carriers across the graphene interface in the out-of-plane direction are still unknown [16, 48, 66]. To study the thermal transport across the atomic-layer interface, a pump-probe method is developed in our lab using MD simulations to calculate the interfacial thermal resistance between graphene nanoribbon (GNR) and silicon crystal. The second generation of Brenner potential [67]: reactive empirical bond order (REBO), based on the Tersoff potential with interactions between C-C bonds, is employed to model the graphene system [68, 69]. The Tersoff potential with interactions between Si-Si bonds is used to model the silicon system. The REBO potential is chosen because its functions and parameters are known to give reasonable predictions of the thermal properties of graphene [21], whereas the adaptive intermolecular reactive empirical bond order (AIREBO) was reported to underestimate the dispersion of ZA phonons in graphene [70]. It has been proposed that the interactions between carbon atoms and the substrate are primarily short-range van der Waals type (vdW) [71, 72]. Therefore, the C-Si couplings are modeled as vdW interactions using the Lennard-Jones (LJ) potential $V(r)=4\varepsilon[(\sigma/r)^{12}-(\sigma/r)^{6}]$, where σ is the distance parameter, ε is the energy parameter, and r is the interatomic distance. The ε parameter determines the strength of the specific interactions between graphene and silicon. In the calculation, ε and σ are set as 8.909 meV and 3.326 Å, respectively [73]. To save computational time, the LJ potential is truncated at a cutoff distance of $r_c=3.5\sigma$. The initial velocities in each direction are extracted from the Gaussian distribution for the given temperature 300 K. At the start of the simulation, the position of the GNR is located 3.7 Å above the upper layer of the Si bulk. A configuration of the system is shown in Figure 5A. Periodic boundary conditions are applied to the x and y directions, and free boundary condition is applied to the z direction. Dimensions of the GNR are smaller than those of the silicon to avoid boundary interactions through the periodic boundaries. The step for time integration is 0.5 fs (1 fs=10^{-15} s). All MD simulations are performed using the large-scale atomic/molecular massively parallel simulator (LAMMPS) package [74].

As shown in Figure 5A, after the MD system reaches thermal equilibrium, an ultrafast heat impulse is applied on the supported GNR. In the heating process, nontranslational kinetic energy is evenly added to the GNR system in each direction by rescaling velocities of atoms. When the excitation is released, the temperature of the GNR (T_{GNR}) will increase dramatically and then gradually reduce during the thermal relaxation process. In our work, three layers of silicon atoms beneath the supported GNR are grouped to calculate the surface temperature of the silicon

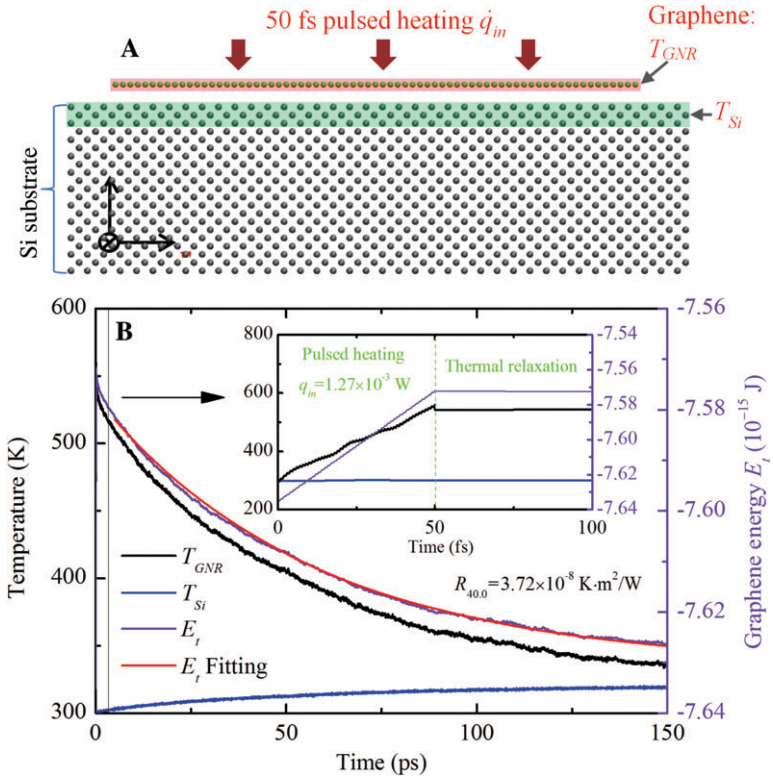

Figure 5: (A) Atomic configuration of the GNR and silicon system. Periodic boundary conditions are applied to the *x* and *y* directions and free boundary condition to the *z* direction. A thermal impulse $\dot{q}_{in}$ is imposed on the supported GNR after thermal equilibrium calculation, and the top three layers of silicon atoms are grouped to calculate the surface temperature of the silicon substrate. (B) Temperature evolutions (left *y* axis) of GNR and Si for 50 fs pulsed thermal excitation and 150 ps thermal relaxation. The overall energy and fitting for the supported GNR system are shown in the right *y* axis. The calculated thermal resistance from this overall fitting method equals 3.72×10^{-8} K·m^2/W. The fitting profile calculated from a single *R* value soundly matches the MD simulation results.

bulk (T_{Si}) as shown in Figure 5A. The T_{GNR}, T_{Si}, and GNR system energy (E_t) are recorded each time step during the thermal relaxation. In the MD simulation, the energy decay of the GNR is only caused by its thermal energy loss to the silicon system. Therefore, given the energy and temperature evolution of the graphene system, the interfacial thermal resistance (R) between the supported GNR and silicon substrate can be calculated using the equation

$$\frac{\partial E_t}{\partial t} = \frac{T_{GNR} - T_{Si}}{R/A} \quad (1)$$

where E_t is the system's energy of the supported GNR, and A is GNR's area. Instant R results can be calculated at each time step according to the local energy-changing rate and corresponding temperature difference. We have tried this method and found that it is subject to the noise in the energy decay, and the calculated interface thermal resistance has a very large uncertainty. If R has little variation within the temperature range during thermal relaxation, a constant R value can be substituted into Eq. (1) to predict the E_t profiles. Under such scenario, the interfacial thermal resistance can be calculated by fitting the E_t profile using the least square method based on an integral form of Eq. (1) as detailed in the next section.

To understand the thermal transport across the graphene and substrate interface, a silicon crystal with dimensions of 5.8×40.0×5.4 nm^3 (x×y×z) is built. The size of the supported GNR is 4.1×38.5 nm^2 (x×y). After 300 ps canonical ensemble (NVT) and 100 ps microcanonical ensemble (NVE) calculation, the whole system reaches thermal equilibrium at 300 K. Then, the GNR is exposed to a thermal impulse of $\dot{q}_{in}$=1.27×10^{-3} W for 50 fs. After excitation, T_{GNR} increases to 559.7 K, and the adjacent silicon surface temperature T_{Si} is 299.4 K as shown in Figure 5B. In the following 150-ps thermal relaxation process, energy dissipation from graphene to the silicon substrate is recorded, and the interfacial thermal resistance is calculated. The equilibrium distance between graphene and Si-substrate surface is 3.2 Å based on the modeling. The energy and temperature results are averaged over 100 steps in the calculation to suppress noise. Temperature evolutions and energy fitting results are shown in Figure 5B. It is observed that after the 50-fs thermal excitation is released, the energy of the graphene goes down quickly

due to the energy transfer to the Si substrate. At the same time, the graphene temperature also goes down accordingly, and a slight temperature rise is observed for the silicon atoms adjacent to the interface. The energy decay fitting in Figure 5B is performed based on Eq. (1) and takes the integral form as $E_t = E_0 + (R/A)\cdot\int_0^t (T_{GNR} - T_{Si})dt$. Here, R is treated constant, and such assumption will be discussed and validated later. E_0 is graphene's initial energy.

The calculated thermal resistance $R_{40.0}$ equals 3.72×10^{-8} K·m²/W, which is in the same magnitude with previous studies of graphene on 6H-SiC and SiO_2 [28, 53]. At the beginning of the thermal relaxation process, a faster decay in GNR's total energy is observed. This is caused by the strong energy disturbance induced by the thermal impulse to the system. During that period, the potential and kinetic energies have not yet reached equilibrium. Therefore, the initial part (5 ps) of the thermal relaxation profile is strongly dominated by the energy transfer from kinetic to potential energy in graphene and is excluded from the fitting process. It can be observed from Figure 5B that the fitting curve soundly matches the energy profile using a constant $R_{40.0}$. This leads to a strong conclusion that the interfacial thermal resistance between GNR and Si does not have large change over the relaxation temperature of 300–500 K.

To further assess the validity of the overall fitting method with a constant R, a new case with GNR's dimensions of 4.1×18.3 nm² ($x\times y$) is built. The silicon substrate used is 5.8×20.0×5.4 nm³ ($x\times y\times z$). In this case, the heating rate $\dot{q}_{in} = 6.04\times10^{-4}$ W, and both overall and instant R values are calculated and compared. The overall fitting results using integration is shown in Figure 6A, and R is calculated at 3.52×10^{-8} K·m²/W. As the energy decay is driven by the temperature difference $\Delta T = T_{GNR} - T_{Si}$, in Figure 6B, we plot out how the graphene energy changes against $\int_0^t \Delta T dt$. It is observed that the E_t profile has a linear relation with $\int_0^t \Delta T dt$, which further proves the fact that the thermal resistance R is nearly constant during the relaxation process. In fact, we can use this profile to determine the interfacial thermal resistance. The E_t profile is divided into many segments as shown in Figure 6B. For each segment (t_1 to t_2), R can be treated constant and can be determined by linear fitting of the curve in Figure 6B. The fitted slope equals A/R and can be used to determine R. The calculated results are shown in Figure 6C. It is observed that the instant R values vary around the overall fitting results $R_{20.0}$. From the above discussions, it is safe to conclude that the overall integration fitting method is accurate enough to be used in the pump-probe method.

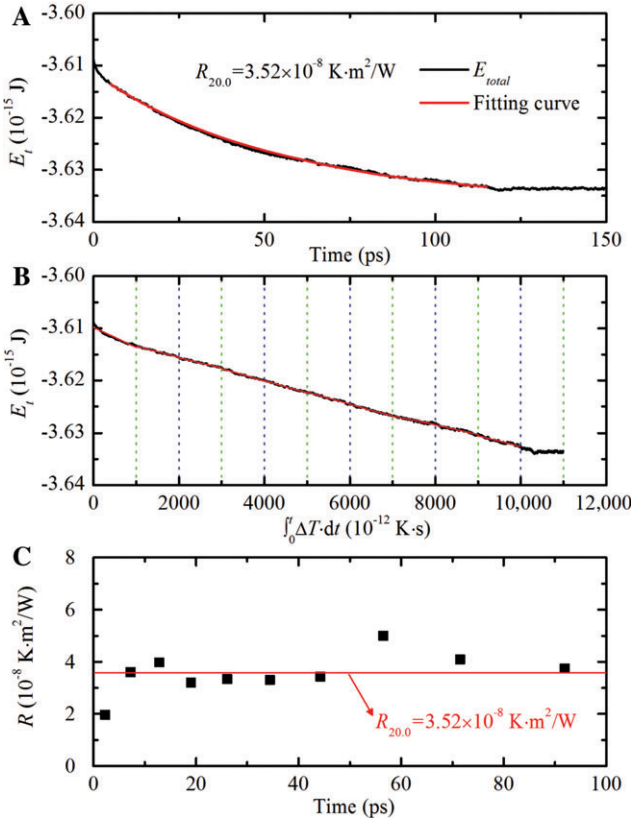

Figure 6: Comparisons of the overall fitting result and instant R calculation results. Size of the GNR is 4.1×18.3 nm² ($x\times y$). By integrating the temperature differences between T_{GNR} and T_{Si}, the energy relaxation profile of GNR can be correlated to $\Delta T dt$ directly and slope of the profile can be linearly fitted to calculate the segment interfacial thermal resistance values, which is around the overall fitting results.

5.2 Phonon mode energy decay and thermal rectification discussion

In the preceding discussions, it has been mentioned that the presence of a substrate will significantly affect the thermal transport in graphene due to the damping of ZA phonons. The thermal conductivity of supported graphene is suppressed due to the strong phonon coupling at the interface. To obtain an insightful understanding of this problem, the decomposed energies for each phonon mode is evaluated for a 4.1×38.5-nm² supported GNR. The energy is normalized to a nominal temperature defined as $E_i/(1/2)k_B$ with unit K and is used to present the energy values in each direction. Here, E_i is the kinetic energy in the direction i (i=x, y or z), and k_B is the Boltzmann constant. Energy evolutions for the thermal relaxation process are shown in Figure 7. The nominal temperatures of the three phonon modes are around the same value of 550 K at the beginning point (t=0) of the thermal relaxation process

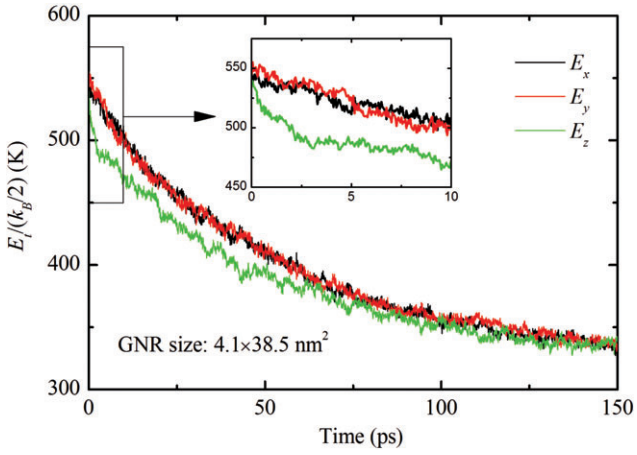

Figure 7: Phonon energy evolutions in the supported GNR system. It is observed that E_z decreases faster than E_x and E_y in the early stage, indicating a much stronger exchange between kinetic and potential energies for ZA phonons in graphene than the LA and TA phonons.

(inset of Figure 7). However, it is noticed that there is a quick drop of E_z when the thermal excitation is released. This is largely caused by the stronger coupling between the kinetic energy and potential energy for out-of-plane movements. Owing to the relative lower energy of the ZA phonons, the in-plane longitudinal (LA) and transverse (TA) phonons will keep transferring thermal energy to ZA phonons until the energy difference is gone. This can be seen from the decreasing energy gaps between E_x, E_y and E_z along the relaxation process. The energy coupling rates among different phonon modes have been discussed in our previous study on energy inversion in graphene [75]. At nominal temperature 80 K, the phonon relaxation time among in-plane and out-of-plane phonons is 4.7 times larger than that between in-plane phonons, meaning the energy transfer for LA→ZA and TA→ZA are much slower than that between LA and TA.

Thermal rectification has been found in asymmetric graphene nanoribbons with different chirality [15, 76–79]. However, up to date, the thermal rectification between supported graphene and its substrate has not yet been studied. To explore this important thermal phenomenon, a silicon substrate with dimensions of 5.8×10.2×5.4 nm^3 (x×y×z) is built, and the supported GNR is 4.1×8.6 nm^2 (x×y). After the system reaches thermal equilibrium at 300 K, a heat impulse $\dot{q}_{in}$=2.84×10^{-4} W is imposed on the GNR system and by fitting the GNR's energy relaxation profile, the interfacial thermal resistance is calculated at 3.31×10^{-8} K·m^2/W. In this process, the energy is transferred from the heated graphene to the silicon substrate. To investigate the thermal rectification across the graphene-Si interface, two more cases are calculated with different initial system temperatures. The equilibrium temperature for the first case is 400 K. After the thermal equilibrium calculation, thermal energy is removed from the GNR system for 50 fs with a cooling rate $\dot{q}_{out}$=-2.48×10^{-4} W, and T_{GNR} drops to 175 K at the end of the cooling process. The interfacial thermal resistance (R) is calculated at 3.20×10^{-8} K·m^2/W based on global data fitting. This R value is only 3% lower than that of the case with T_{GNR}>T_{Si}. For the second case, the initial system temperature is set at 350 K. After cooling the supported GNR with $\dot{q}_{out}$=1.24×10^{-4} W for 50 fs, T_{GNR} decreases to 250 K. Following the same calculation procedure, the interfacial thermal resistance is calculated at 3.62×10^{-8} K·m^2/W, which is 9% higher than that of the case with T_{GNR}>T_{Si}. It has been observed in the above discussions that the thermal resistance between graphene and the Si substrate do not have substantial changes against temperature, indicating that the thermal resistance for the cases with T_{GNR}<T_{Si} will be around the same values as the above two cases. Considering the calculation uncertainty, the difference between the heating (T_{GNR}>T_{Si}) and cooling (T_{GNR}<T_{Si}) cases are very small. It is safe to conclude that there is no thermal rectification phenomenon in thermal transport across the graphene and silicon interface.

5.3 Size effect on graphene's interfacial thermal resistance

The size dependence of thermal conductivity has been reported in various low-dimensional nanomaterials [75, 80–83]. As a novel 2D material, it is found that the thermal conductivity of suspended graphene and graphene nanoribbons (GNR) is also size dependent [84, 85]. The length effect on the thermal conductivity of graphene is due to its intrinsically long phonon mean free path, which is up to 775 nm at room temperature [66]. The confined dimension in the lateral directions of supported graphene will greatly affect the phonon behaviors at the graphene-substrate interface. Therefore, it is of great interest to investigate the effects of dimension on the interfacial thermal resistance between graphene and silicon.

To study the size effect on the interfacial thermal resistance, we fix the GNR's width at 4.1 nm and substrate thickness at 5.4 nm. Supported GNRs with lengths of 1.6, 2.7, 8.6, 18.3, 38.5, and 78.2 nm are designed and studied. The thermal resistance results calculated using the pump-probe method are shown in Figure 8A. It can be observed from Figure 8A that the length of the supported GNR has significant impact on the interfacial thermal resistance between GNR and Si at short length scales from 0 to 40 nm. When the length is larger than 40 nm, the calculated R

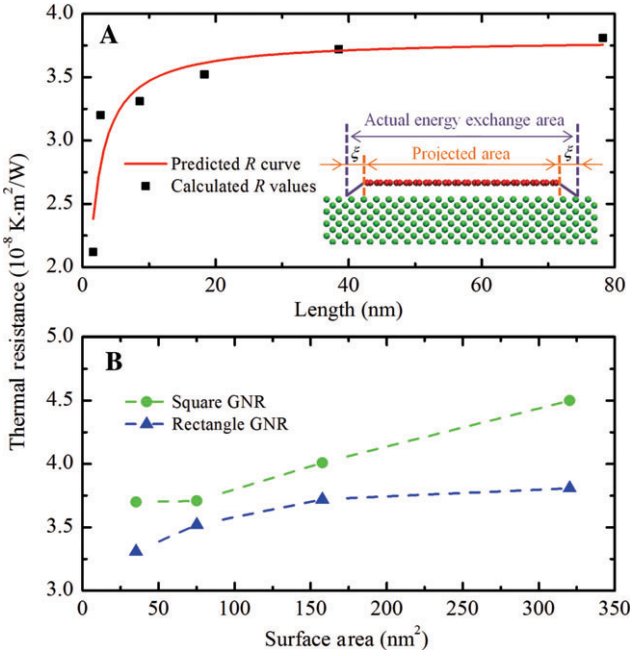

Figure 8: Effect of graphene dimension on the interfacial thermal resistance between GNR and Si. (A) When the length of the supported GNR becomes longer, the interfacial thermal resistance becomes larger due to the reduced edge effect. The inset shows 1) the projected area of graphene for thermal resistance evaluation, and 2) the actual energy exchange area that is strongly affected by the interaction between GNR and Si. This area is larger than the projected area. (B) Square-shaped GNR has larger thermal resistance values than the rectangle-shaped GNR.

tends to converge to a constant value. To elucidate this length effect, the actual energy exchange area on the Si substrate is explored. It was mentioned above that the cutoff distance between carbon and silicon atoms is set as 3.5 σ, which is 11.641 Å in all cases. The equilibrium distance between GNR and Si substrate surface is ~3.2 Å. This indicates that the actual surface areas involved in the thermal transport process are larger than the projected GNR areas on the Si substrate, which is used in the overall fitting method to calculate the interfacial thermal resistance. This phenomenon is explained in the inset in Figure 8A. The relation between the thermal resistance (R) calculated using the overall fitting method and the ideal one (R_{real}) without the edge effect is expressed as

$$R=\frac{R_{real}\cdot W\cdot L}{(W+\xi)(L+\xi)}, \quad (2)$$

where W and L are the width and length of the supported GNR, respectively, and ξ is the effective distance extended from the edge of the projected area, as is shown in the inset of Figure 8A. Such area extension is caused by the long-range vdW interaction. The interatomic forces in the extended areas are much weaker compared to those in the projected areas, making us believe that ξ is smaller than 3.5 σ. On the other hand, the contributions from the extended areas cannot be neglected when the surface area of the supported GNR is small. Given the calculated thermal resistance values, we use Eq. (2) to fit the results shown in Figure 8A to determine R_{real} and ξ. The ideal interfacial thermal resistance without the edge effect is determined at 4.68×10^{-8} K·m²/W, and ξ is determined at 9.5 Å. The ξ value determined here is close to, and a little smaller than, the cutoff distance used in the calculation (11.641 Å), confirming our above prediction about the size effect.

In the above calculations, the supported GNRs are all rectangle shaped. To compare the effects of GNR's formation on the interfacial thermal resistance, square-shaped GNRs with the same surface areas are built, and the results are shown in Figure 8B. It is evident that the interfacial thermal resistances of rectangle-shaped GNRs are smaller than those of square-shaped ones. It is ready to prove that under the same surface area, the rectangle formations have larger perimeters than the square formations. Therefore, both the phonon boundary scatterings and the effective thermal contact areas in the rectangle-shaped GNRs will be larger than those in the square-shaped GNRs, which will increase the phonon energy decay rate and lead to a smaller thermal resistance. We calculated that the extended distance ξ from the edges of supported GNR is 9.5 Å. Therefore, the effective thermal contact areas for both shapes can be calculated, and the thermal resistance for the square-shaped GNRs can be predicted. Take the 4.1×38.5-nm² GNR as an example, its interfacial thermal resistance is 3.72×10^{-8} K·m²/s. The square-shaped GNR with the same surface area has a dimension 12.59×12.59 nm². After adding ξ to the width and length calculation, their effective thermal contact area ratio $A_{eff,rec}/A_{eff,squ}$ is calculated at 1.09. Based on this ratio, the thermal resistance for the square-shaped GNR can be predicted at 4.04×10^{-8} K·m²/s. This prediction is very close to the calculated result 4.01×10^{-8} K·m²/s by direct MD simulation, which further proves the validity of the effective surface area analysis. One argument would arise that the size of the supported graphene will affect the phonon mean free path, which then will affect the phonon coupling between graphene and Si. We expect this speculation would hold and be more visible for larger-size graphenes. In our calculation, the graphene size is very small (4.1 nm width for the rectangular one), so the phonon mean free path in graphene is already significantly suppressed and does not have strong/visible size effect on the phonon coupling between graphene and Si.

5.4 Surface roughness' effect on interfacial thermal resistance

In our previous work, we reported for the first time that by introducing sub-nm roughness on a silicon surface, the energy coupling between a single layer graphene and the Si substrate can be improved substantially [62]. To study the effect of the surface roughness on interfacial thermal transport, a 4.1×18.3-nm^2 (x×y) graphene nanoribbon (GNR) was built and placed on a silicon substrate with dimensions of 5.8×20.0×5.4 nm^3 (x×y×z). Configuration of the system is the same as in Figure 5A. Combinations of the surface roughness patterns are countless. In this work, a zebra-stripe pattern is used, and variations are made by changing the groove depth δ. Consistency for comparisons is achieved by placing all grooves in the x direction of the Si substrate. The separation distance of the neighboring grooves is ~2.0 nm, which is the same as the width for each groove. Figure 9A–C show the atomic configurations of the systems after thermal equilibrium. Free boundary condition is applied to the out-of-plane direction, and periodic boundary conditions are applied to the in-plane directions. It is observed that when δ=0.54 nm, the graphene is bent to fit the Si substrate surface, and both the supported and suspended areas are in close contact with Si. For δ=0.68 nm, most of the suspended graphene area remains in close contact with the Si substrate but is partially separated from Si. For the δ=0.81 nm case, all the suspended areas of the graphene are separated from the Si substrate. The reasons for such differences will be elucidated in the following discussions. Take the δ=2.0 nm case as an example, after 300 ps NVT and 100 ps NVE calculations, the whole system reaches a thermal equilibrium at 300 K. Then, a thermal impulse of $\dot{q}_{in}$=6.0×10^{-4} W is applied to the supported GNR for 50 fs. The whole system is then left for thermal relaxation under NVE calculation for another 150 ps. The calculated thermal resistance ($R_{\delta=2.0\ \mathrm{nm}}$) is 4.42×10^{-8} K·m^2/W, 26% larger than the flat surface case under the same conditions.

To investigate the interfacial thermal resistance relation with surface roughness, variations have been made on the groove depth δ and cases of δ=0.27, 0.54, 0.68, 0.81, 1.09, 1.49, and 2.0 nm are studied. Groove depths larger than 2.0 nm are not studied because the cutoff distance for the 12-6 LJ potential is only 1.16 nm. Therefore, it is safe to speculate that the thermal resistance values will not change substantially for δ>2.0 nm. The calculated thermal resistance is shown in Figure 9D against the groove depth. For the results in Figure 9D, the real areas of the graphene, not their projected areas on the Si substrate, are used for resistance evaluation. It is very surprising and interesting to observe

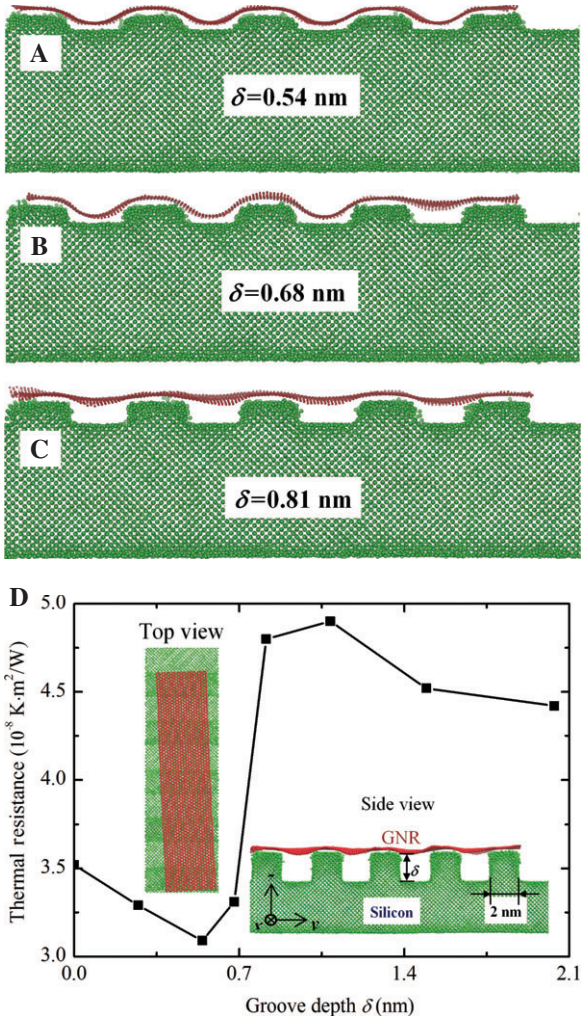

Figure 9: (A–C) Atomic configurations for δ=0.54, δ=0.68, and δ=0.81 nm cases. (D) Interfacial thermal resistance variation against surface roughness/groove depth. Top and side views of the δ=2.0 nm case are depicted in the insets. Reproduced with permission from Reference [38]. The Royal Society of Chemistry, Copyright (2013).

that the interfacial thermal resistance first decreases as δ becomes larger when the groove depth is smaller than 7 Å. R reaches the lowest value of 3.09×10^{-8} K·m^2/W when δ is 5.4 Å. This is contrary to the traditional thought that, in comparison with a flat surface, a rough surface should always give a larger interfacial thermal resistance due to the poor contact. To explain this new finding, the interatomic forces between graphene and silicon are calculated for the δ=0.54 nm case, and the results are shown in Figure 10A. The supported and suspended areas are cross-adjacent, and each region has a width of 2.0 nm. Owing to the roughness of the silicon surface, the interatomic forces are not evenly distributed in the supported graphene. For graphene over the groove, most of the C-Si distance is large, beyond the repulsive force range. So the C-Si interaction

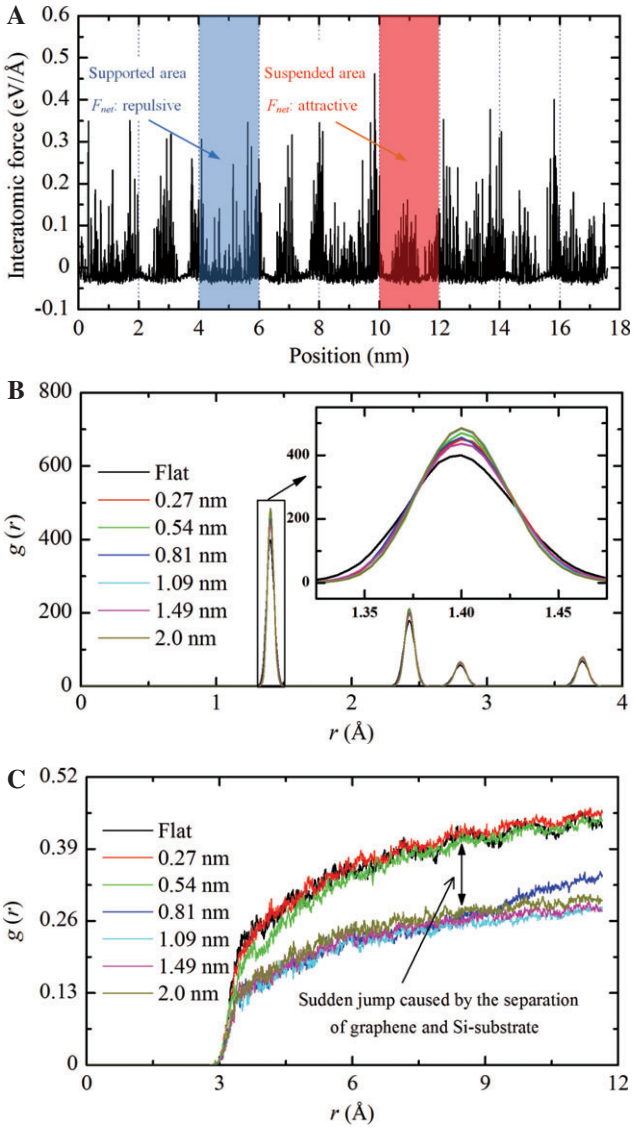

Figure 10: (A) Interatomic forces between supported GNR and δ=0.54 nm dented silicon substrate. The blue and red shaded areas indicate the supported and suspended GNR regions respectively. (B) Radial distribution functions for the supported GNRs. The peaks are sharper for the dented Si cases, indicating stretching in graphene. (C) Radial distribution functions between graphene and Si substrate. The $g(r)$ values drop to significant lower levels when the groove depth δ becomes larger than 0.81 nm. This explains the sudden thermal resistance increase from δ=0.51 nm to δ=0.81 nm observed in Figure 9D. Reproduced with permission from Reference [38]. The Royal Society of Chemistry, Copyright (2013).

is attractive. When the groove depth is small, this attractive force is strong enough to bend the graphene to fit the silicon surface. As the overall force on the graphene will be zero in average, a net repulsive force will arise for the supported graphene areas. For example, at the location 4~6 nm in the length direction of the GNR (shown in Figure 10A) the graphene is supported, and the net interatomic force is calculated at +1.17 eV/Å. The positive sign indicates a repulsive force. This force gives a pressure of 228 MPa for the supported graphene. Such very high pressure will significantly reduce the local interfacial thermal resistance. At the location of 10~12 nm shown in Figure 10A, the graphene is suspended. The net force is -2.36 eV/Å, and the negative sign indicates an attractive force. The contact pressure between the graphene and Si substrate increases greatly in the supported graphene region due to the significant attractive force in the suspended regions. This is like the supported graphene region is pulled down on both sides by the attractive force in the suspended regions. The significantly increased contact pressure in the supported graphene region leads to a decreased thermal resistance between graphene and silicon. This thermal resistance decrease offsets the thermal resistance increase in the suspended region, giving an overall thermal resistance decrease.

From the above discussion, it is realized that the graphene is kind of stretched by the attractive force in the suspended region and repulsive force in the supported region. Such stretching could be reflected by the structure of the graphene. The radial distribution function (RDF) of the GNRs is calculated, and the results are shown in Figure 10B. As all the GNRs share the same structure, their RDFs give the same formation for all cases. However, detailed inspections reveal that the peaks become narrower and sharper when GNRs are supported on the dented Si substrate with a larger groove depth. Also, a slight shift of the first peak location to a larger atomic separation is observed. This firmly confirms that the structures of the GNRs on dented Si surface are stretched due to the existence of grooves. For more relaxed GNRs, like that on the flat Si surface, the structure is more relaxed, and the RDF peak has a broader line width.

When δ becomes large enough, in the suspended region, a lot of graphene atoms will have very weak or zero interaction with Si atoms. To elucidate this phenomenon, the RDF between graphene and silicon are calculated, and the results are shown in Figure 10C. It is observed that the $g(r)$ values are evidently larger at small groove depths and drop to a much lower level when δ is increased from 0.54 nm to 0.81 nm. This is corresponding to the jump of the interfacial thermal resistance from δ=0.54 nm to δ=0.81 nm observed in Figure 9D. This again proves the fact that when the groove depth is small, the supported graphene will stay closely with the dented Si surface. When graphene in the suspended region is completely separated from Si (weak/no coupling), the thermal resistance will jump suddenly. At the same time, the repulsive force in the supported area becomes smaller, and the local thermal resistance increases due to the reduced localized pressure.

Therefore, the graphene will hang over the grooves, and the corresponding thermal resistance increases due to significant reduction in thermal contact area.

6 Interfaces beyond graphene and challenges

6.1 Other 2-D materials beyond graphene

Similar 2-D materials beyond graphene, such as silicene [86], hexagonal boron nitride (h-BN), [87] and MoS_2 [88], are attracting more and more attentions. These materials might also possess extraordinary properties as graphene as the structure is similar, while they could feature some different properties due to different chemical composition. Unlike the even surface of graphene, silicene has a buckled honeycomb structure filled with silicon atoms. Recent studies show that the thermal conductivity of silicene is remarkably low compared with the high thermal conductivity of graphene [89–91]. The reason might stem from the buckled structure of silicone, which results in poor ZA mode of phonons and contribute little to thermal transport along the lateral direction. The ZA mode phonons are the main driving force for the high thermal conductivity of graphene [89]. The thermal transport in silicene under various conditions, such as thermal response under stretching [92] and hybrid heterostructure with graphene [93], have been studied. As the in-plane thermal conductivity is abnormally low, the interfacial thermal conductance of silicene interfaces is of great interest to investigate.

MoS_2 is an alternative of graphene that is stable as a layered material with a small band gap (graphene has no band gap) [94]. Therefore, MoS_2 has plenty of potential applications. Besides, MoS_2 has strong Raman excitation [95, 96]. A recent study shows that the thermal conductivity of few-layer MoS_2 measured by Raman thermometry is around 52 W/mK [88]. For h-BN, Jo et al. measured the thermal conductivity of a few layer samples as 230 W/mK by using the microbridge method [87]. Current works are focusing on the thermal transport study of these materials. It is still of great significance to study the thermal transport across these atomic-layer interface materials.

6.2 Challenges in thermal characterization

The experimental study of thermal transport across atomic-layer interfaces still remains a great challenge because of the complicated interface scenarios. As analyzed in the previous sections, the measurement technique needs to have extremely high spatial resolution for temperature probing across atomic-layer interfaces. This can be mediated by using ultrafast techniques. On the other hand, use of metallic coating brings up new issues about the phonon transmission across interfaces. Raman thermometry can be directly employed to measure temperature difference across the interface, while there is resolution limit of spectrometer, which requires temperature difference to be high enough to be sensible. In addition, the high temperature difference induced from the intensive heating might bring additional issue such as morphology modifications from thermal expansions. This issue can be resolved as indicated in the work by Tang et al. that a low temperature difference (just a few degrees) can be probed across the interface [25, 47]. As both techniques have advantages and unsolved issues, we are wondering whether the development of a new technique combining the advantages of ultrafast technique and Raman thermometry will work out in this complicated problem. As the Raman signal is not affected by laser reflections and ultrafast technique features extremely high temporal resolution, we propose that a new technique based on ultrafast Raman thermometry might advance the atomic-layer thermal measurement. Current work is being conducted in Wang's laboratory in this direction.

From the perspective of material properties, the metallic coating (usually coated on top of graphene) would affect the phonon transmission across atomic-layer interfaces as discussed in previous sections. It would be better to study the virgin/original interface without any treatment or coatings to understand the thermal transport of interface materials in real scenario. For CVD-prepared graphene interfaces, the functional groups on graphene have strong impact on the thermal transport across the interface as demonstrated by Hopkins et al. [23]. How to utilize this effect for thermal manipulation, for example, to meet different heat dissipation purpose in different conditions, requires comprehensive understanding on how the functional groups are involved in the phonon transport. This is another area that needs to be focused on by either experimental study or MD simulations. In addition, the complicated morphology of graphene on substrates, such as the wrinkling effect or corrugation problem, does limit the phonon transport across the interface [25]. To what extent and how to prevent this effect need clearer understanding of phonon transmission mechanism, which imposes higher demand on thermal characterization techniques and numerical simulations.

For a highly coupled interface that has a small thermal contact resistance, the temperature difference across the interface becomes very small to measure, and the characterization can be very challenging. In the pump-probe technique, the thermal relaxation time is very short. To recover the exact application scenarios, the effect of various physical and chemistry factors on the graphene-interface energy transport needs to be studied. The heat flow through the interface can be tuned or altered with respect to that of pristine graphene by introducing atomistic alterations of the honeycomb lattice [97]. Such alterations can be achieved through strain [98, 99], folding [100], edge roughness [13–15], grain boundaries [12, 101], vacancies or Stone-Wales defects [102–104], isotopic impurities or substitutional defects [105, 106], and chemical functionalization [11]. It has been proven that by appropriately functionalizing the graphene sheets, it is possible to significantly reduce the Kapitza resistance at the graphene-liquid octane interface [107]. By tuning the vibration modes of the functional groups, the energy coupling between the supported membrane and the substrate can be enhanced. This will, in turn, reduce the thermal contact resistance at the interface.

7 Summary

Targeting the challenges confronted in the study of thermal transport across atomic-layer interfaces, this review discusses the current stage of knowledge in both thermal characterizations and numerical simulations involving thermal transport study of atomic-layer material interfaces. Commonly used techniques, including differential 3ω method, ultrafast pump-probe method, and Raman thermometry with both electrical heating and laser heating methods, were compared and discussed in terms of measurement principle and experimental deployment. The corresponding results obtained by using these techniques in different scenarios are discussed. MD simulations provide an effective pathway to study the physical fundamentals of thermal transport at the atomic scale, the knowledge of which is essential for understanding how energy dissipates across the atomic-layer interface. At the end of this review, the existing challenges and future directions for the thermal characterization of atomic-layer material interfaces are prospected. The combination of the advantages of the pump-probe method and Raman thermometry, which are designated as an ultrafast Raman thermometry technique, should be a good direction for future interfacial thermal transport studies.

Acknowledgments: Y. Y. thanks the financial support from the National Natural Science Foundation of China (No. 51206124) and SRF for ROCS, SEM. X.W thanks for the partial support of this work by the National Science Foundation (CBET1235852), Department of Energy (DENE0000671) and National Natural Science Foundation of China (No. 51428603). We thank Christopher Reilly for careful proofreading of the manuscript.

References

[1] Wu YQ, Ye PD, Capano MA, Xuan Y, Sui Y, Qi M, Cooper JA, Shen T, Pandey D, Prakash G, Reifenberger R. Top-gated graphene field-effect-transistors formed by decomposition of SiC. *Appl. Phys. Lett.* 2008, 92, 092102.

[2] Bolotin KI, Sikes KJ, Hone J, Stormer HL, Kim P. Temperature-dependent transport in suspended graphene. *Phys. Rev. Lett.* 2008, 101, 096802.

[3] Zhang Y, Tan YW, Stormer HL, Kim P. Experimental observation of the quantum hall effect and berry's phase in graphene. *Nature* 2005, 438, 201–204.

[4] Novoselov KS, Geim AK, Morozov SV, Jiang D, Katsnelson MI, Grigorieva IV, Dubonos SV, Firsov AA. Two-dimensional gas of massless Dirac fermions in graphene. *Nature* 2005, 438, 197–200.

[5] Novoselov KS, Geim AK, Morozov SV, Jiang D, Zhang Y, Dubonos SV, Grigorieva IV, Firsov AA. Electric field effect in atomically thin carbon films. *Science* 2004, 306, 666–669.

[6] Du X, Skachko I, Barker A, Andrei EY. Approaching ballistic transport in suspended graphene. *Nat. Nanotechnol.* 2008, 3, 491–495.

[7] Balandin AA, Ghosh S, Bao W, Calizo I, Teweldebrhan D, Miao F, Lau CN. Superior thermal conductivity of single-layer graphene. *Nano Lett.* 2008, 8, 902–907.

[8] Chen S, Wu Q, Mishra C, Kang J, Zhang H, Cho K, Cai W, Balandin AA, Ruoff RS. Thermal conductivity of isotopically modified graphene. *Nat. Mater.* 2012, 11, 203–207.

[9] Lee JU, Yoon D, Kim H, Lee SW, Cheong H. Thermal conductivity of suspended pristine graphene measured by Raman spectroscopy. *Phys. Rev. B* 2011, 83, 081419.

[10] Chen S, Moore AL, Cai W, Suk JW, An J, Mishra C, Amos C, Magnuson CW, Kang J, Shi L. Raman measurements of thermal transport in suspended monolayer graphene of variable sizes in vacuum and gaseous environments. *ACS Nano* 2010, 5, 321–328.

[11] Chien SK, Yang YT, Chen CK. Influence of chemisorption on the thermal conductivity of graphene nanoribbons. *Carbon* 2012, 50, 421–428.

[12] Bagri A, Kim SP, Ruoff RS, Shenoy VB. Thermal transport across twin grain boundaries in polycrystalline graphene from non-equilibrium molecular dynamics simulations. *Nano Lett.* 2011, 11, 3917–3921.

[13] Hu JN, Schiffli S, Vallabhaneni A, Ruan XL, Chen YP. Tuning the thermal conductivity of graphene nanoribbons by edge passivation and isotope engineering: a molecular dynamics study. *Appl. Phys. Lett.* 2010, 97, 133107.

[14] Evans WJ, Hu L, Keblinski P. Thermal conductivity of graphene ribbons from equilibrium molecular dynamics: effect of ribbon width, edge roughness, and hydrogen termination. *Appl. Phys. Lett.* 2010, 96, 203112.
[15] Hu JN, Ruan XL, Chen YP. Thermal conductivity and thermal rectification in graphene nanoribbons: a molecular dynamics study. *Nano Lett.* 2009, 9, 2730–2735.
[16] Zhang JC, Huang XP, Yue YN, Wang JM, Wang XW. Dynamic response of graphene to thermal impulse. *Phys. Rev. B* 2011, 84, 235416.
[17] Reina A, Jia X, Ho J, Nezich D, Son H, Bulovic V, Dresselhaus MS, Kong J. Large area, few-layer graphene films on arbitrary substrates by chemical vapor deposition. *Nano Lett.* 2008, 9, 30–35.
[18] Emtsev KV, Bostwick A, Horn K, Jobst J, Kellogg GL, Ley L, McChesney JL, Ohta T, Reshanov SA, Rohrl J, Rotenberg E, Schmid AK, Waldmann D, Weber HB, Seyller T. Towards wafer-size graphene layers by atmospheric pressure graphitization of silicon carbide. *Nat. Mater.* 2009, 8, 203–207.
[19] Meric I, Han MY, Young AF, Ozyilmaz B, Kim P, Shepard KL. Current saturation in zero-bandgap, top-gated graphene field-effect transistors. *Nat. Nanotechnol.* 2008, 3, 654–659.
[20] Seol JH, Jo I, Moore AL, Lindsay L, Aitken ZH, Pettes MT, Li X, Yao Z, Huang R, Broido D, Mingo N, Ruoff RS, Shi L. Two-dimensional phonon transport in supported graphene. *Science* 2010, 328, 213–216.
[21] Yue Y, Zhang J, Wang X. Micro/nanoscale spatial resolution temperature probing for the interfacial thermal characterization of epitaxial graphene on 4H-SiC. *Small* 2011, 7, 3324–3333.
[22] Zhang CW, Zhao WW, Bi KD, Ma J, Wang JL, Ni ZH, Ni ZH, Chen YF. Heat conduction across metal and nonmetal interface containing imbedded graphene layers. *Carbon* 2013, 64, 61–66.
[23] Hopkins PE, Baraket M, Barnat EV, Beechem TE, Kearney SP, Duda JC, Robinson JT, Walton SG. Manipulating thermal conductance at metal–graphene contacts via chemical functionalization. *Nano Lett.* 2011, 12, 590–595.
[24] Riedl C, Starke U, Bernhardt J, Franke M, Heinz K. Structural properties of the graphene-SiC(0001) interface as a key for the preparation of homogeneous large-terrace graphene surfaces. *Phys. Rev. B* 2007, 76, 245406.
[25] Tang X, Xu S, Zhang J, Wang X. Five orders of magnitude reduction in energy coupling across corrugated graphene/substrate interfaces. *ACS Appl. Mater. Interf.* 2014, 6, 2809–2818.
[26] Ismach A, Druzgalski C, Penwell S, Schwartzberg A, Zheng M, Javey A, Bokor J, Zhang Y. Direct chemical vapor deposition of graphene on dielectric surfaces. *Nano Lett.* 2010, 10, 1542–1548.
[27] Schmidt AJ, Collins KC, Minnich AJ, Chen G. Thermal conductance and phonon transmissivity of metal-graphite interfaces. *J. Appl. Phys.* 2010, 107, 104907.
[28] Chen Z, Jang W, Bao W, Lau CN, Dames C. Thermal contact resistance between graphene and silicon dioxide. *Appl. Phys. Lett.* 2009, 95, 161910.
[29] Mirmira S, Fletcher L. Review of the thermal conductivity of thin films. *J. Thermophys. Heat Transf.* 1998, 12, 121–131.
[30] Zhang X, Grigoropoulos CP. Thermal conductivity and diffusivity of free-standing silicon nitride thin films. *Rev. Sci. Instrum.* 1995, 66, 1115–1120.
[31] Powell R. Experiments using a simple thermal comparator for measurement of thermal conductivity, surface roughness and thickness of foils or of surface deposits. *J. Sci. Instrum.* 1957, 34, 485.
[32] Völklein F. Thermal conductivity and diffusivity of a thin film sio2, si3n4 sandwich system. *Thin Solid Films* 1990, 188, 27–33.
[33] Cahill DG, Fischer HE, Klitsner T, Swartz E, Pohl R. Thermal conductivity of thin films: measurements and understanding. *J. Vacuum Sci. Technol. A* 1989, 7, 1259–1266.
[34] Käding O, Skurk H, Goodson K. Thermal conduction in metallized silicon-dioxide layers on silicon. *Appl. Phys. Lett.* 1994, 65, 1629–1631.
[35] Redondo A, Beery JG. Thermal conductivity of optical coatings. *J. Appl. Phys.* 1986, 60, 3882–3885.
[36] Wang X, Hu H, Xu X. Photo-acoustic measurement of thermal conductivity of thin films and bulk materials. *J. Heat Transf.* 2001, 123, 138–144.
[37] Ohta H, Shibata H, Waseda Y. New attempt for measuring thermal diffusivity of thin films by means of a laser flash method. *Rev. Sci. Instrum.* 1989, 60, 317–321.
[38] Swartz E, Pohl R. Thermal resistance at interfaces. *Appl. Phys. Lett.* 1987, 51, 2200–2202.
[39] Borca-Tasciuc T, Kumar A, Chen G. Data reduction in 3ω method for thin-film thermal conductivity determination. *Rev. Sci. Instrum.* 2001, 72, 2139–2147.
[40] Cahill DG, Goodson K, Majumdar A. Thermometry and thermal transport in micro/nanoscale solid-state devices and structures. *J. Heat Transf.* 2002, 124, 223–241.
[41] Nair R, Blake P, Grigorenko A, Novoselov K, Booth T, Stauber T, Peres N, Geim A. Fine structure constant defines visual transparency of graphene. *Science* 2008, 320, 1308–1308.
[42] Mak KF, Shan J, Heinz TF. Seeing many-body effects in single- and few-layer graphene: observation of two-dimensional saddle-point excitons. *Phys. Rev. Lett.* 2011, 106, 046401.
[43] Mak KF, Lui CH, Heinz TF. Measurement of the thermal conductance of the graphene/SiO2 interface. *Appl. Phys. Lett.* 2010, 97, 221904.
[44] Hsu IK, Kumar R, Bushmaker A, Cronin SB, Pettes MT, Shi L, Brintlinger T, Fuhrer MS, Cumings J. Optical measurement of thermal transport in suspended carbon nanotubes. *Appl. Phys. Lett.* 2008, 92, 063119–063119-3.
[45] Calizo I, Balandin A, Bao W, Miao F, Lau C. Temperature dependence of the Raman spectra of graphene and graphene multilayers. *Nano Lett.* 2007, 7, 2645–2649.
[46] Cai W, Moore AL, Zhu Y, Li X, Chen S, Shi L, Ruoff RS. Thermal transport in suspended and supported monolayer graphene grown by chemical vapor deposition. *Nano Lett.* 2010, 10, 1645–1651.
[47] Tang X, Xu S, Wang X. Corrugated epitaxial graphene/SiC interfaces: photon excitation and probing. *Nanoscale* 2014, 6, 8822–8830.
[48] Koh YK, Bae MH, Cahill DG, Pop E. Heat conduction across monolayer and few-layer graphenes. *Nano Lett.* 2010, 10, 4363–4368.
[49] Chen CC, Li Z, Shi L, Cronin SB. Thermal interface conductance across a graphene/hexagonal boron nitride heterojunction. *Appl. Phys. Lett.* 2014, 104, 081908.
[50] Wang HX, Gong JX, Pei YM, Xu ZP. Thermal transfer in graphene-interfaced materials: contact resistance and interface engineering. *ACS Appl. Mater. Interf.* 2013, 5, 2599–2603.
[51] Landry ES, McGaughey AJH. Thermal boundary resistance predictions from molecular dynamics simulations and theoretical calculations. *Phys. Rev. B* 2009, 80, 165304.

[52] Zhang J, Wang X. Thermal transport in bent graphene nanoribbons. *Nanoscale* 2013, 5, 734–743.
[53] Xu ZP, Buehler MJ. Heat dissipation at a graphene-substrate interface. *J. Phys. Condens. Mat.* 2012, 24, 47530.
[54] Wei ZY, Ni ZH, Bi KD, Chen MH, Chen YF. Interfacial thermal resistance in multilayer graphene structures. *Phys. Lett. A* 2011, 375, 1195–1199.
[55] Persson BNJ, Ueba H. Heat transfer between weakly coupled systems: graphene on a-sio2. *Europhys. Lett.* 2010, 91, 56001.
[56] Luo TF, Lloyd JR. Non-equilibrium molecular dynamics study of thermal energy transport in Au-SAM-Au junctions. *Int. J. Heat Mass. Tran.* 2010, 53, 1–11.
[57] Zhong HL, Lukes JR. Interfacial thermal resistance between carbon nanotubes: molecular dynamics simulations and analytical thermal modeling. *Phys. Rev. B* 2006, 74, 125403.
[58] Muller Plathe F. A simple nonequilibrium molecular dynamics method for calculating the thermal conductivity. *J. Chem. Phys.* 1997, 106, 6082–6085.
[59] Schmidt AJ, Chen XY, Chen G. Pulse accumulation, radial heat conduction, and anisotropic thermal conductivity in pump-probe transient thermoreflectance. *Rev. Sci. Instrum.* 2008, 79, 114902.
[60] Lyeo HK, Cahill DG. Thermal conductance of interfaces between highly dissimilar materials. *Phys. Rev. B* 2006, 73, 144301.
[61] Stoner RJ, Maris HJ. Kapitza conductance and heat-flow between solids at temperatures from 50 to 300 k. *Phys. Rev. B* 1993, 48, 16373–16387.
[62] Zhang J, Wang Y, Wang X. Rough contact is not always bad for interfacial energy coupling. *Nanoscale* 2013, 5, 11598–11603.
[63] Cheeke JDN, Ettinger H, Hebral B. Analysis of heat-transfer between solids at low-temperatures. *Can. J. Phys.* 1976, 54, 1749–1771.
[64] Little WA. The transport of heat between dissimilar solids at low temperatures. *Can. J. Phys.* 1959, 37, 334–349.
[65] Swartz ET, Pohl RO. Thermal-boundary resistance. *Rev. Mod. Phys.* 1989, 61, 605–668.
[66] Ghosh S, Calizo I, Teweldebrhan D, Pokatilov E, Nika D, Balandin A, Bao W, Miao F, Lau CN. Extremely high thermal conductivity of graphene: prospects for thermal management applications in nanoelectronic circuits. *Appl. Phys. Lett.* 2008, 92, 151911.
[67] Brenner DW, Shenderova OA, Harrison JA, Stuart SJ, Ni B, Sinnott SB. A second-generation reactive empirical bond order (REBO) potential energy expression for hydrocarbons. *J. Phys. Condens. Mat.* 2002, 14, 783.
[68] Tersoff J. Empirical interatomic potential for carbon, with applications to amorphous carbon. *Phys. Rev. Lett.* 1988, 61, 2879.
[69] Dodson BW. Development of a many-body Tersoff-type potential for silicon. *Phys. Rev. B* 1987, 35, 2795.
[70] Lindsay L, Broido D. Optimized Tersoff and Brenner empirical potential parameters for lattice dynamics and phonon thermal transport in carbon nanotubes and graphene. *Phys. Rev. B* 2010, 81, 205441.
[71] Hertel T, Walkup RE, Avouris P. Deformation of carbon nanotubes by surface van der Waals forces. *Phys. Rev. B* 1998, 58, 13870.
[72] Xiao J, Dunham S, Liu P, Zhang Y, Kocabas C, Moh L, Huang Y, Hwang KC, Lu C, Huang W. Alignment controlled growth of single-walled carbon nanotubes on quartz substrates. *Nano Lett.* 2009, 9, 4311–4319.
[73] Ong ZY, Pop E. Molecular dynamics simulation of thermal boundary conductance between carbon nanotubes and SiO2. *Phys. Rev. B* 2010, 81, 155408.
[74] Plimpton S. Fast parallel algorithms for short-range molecular dynamics. *J. Computat. Phys.* 1995, 117, 1–19.
[75] Chang C, Okawa D, Garcia H, Majumdar A, Zettl A. Nanotube phonon waveguide. *Phys. Rev. Lett.* 2007, 99, 045901.
[76] Yang N, Zhang G, Li B. Thermal rectification in asymmetric graphene ribbons. *Appl. Phys. Lett.* 2009, 95, 033107.
[77] Cheh J, Zhao H. Thermal rectification in asymmetric u-shaped graphene flakes. *J. Stat. Mech. Theory Exp.* 2012, 2012, P06011.
[78] Zhang G, Zhang H. Thermal conduction and rectification in few-layer graphene y junctions. *Nanoscale* 2011, 3, 4604–4607.
[79] Gunawardana K, Mullen K, Hu J, Chen YP, Ruan X. Tunable thermal transport and thermal rectification in strained graphene nanoribbons. *Phys. Rev. B* 2012, 85, 245417.
[80] Maruyama S. A molecular dynamics simulation of heat conduction in finite length SWNTs. *Physica. B. Condens. Matter* 2002, 323, 193–195.
[81] Yang N, Zhang G, Li B. Violation of Fourier's law and anomalous heat diffusion in silicon nanowires. *Nano Today* 2010, 5, 85–90.
[82] Zhang G, Li B. Thermal conductivity of nanotubes revisited: effects of chirality, isotope impurity, tube length, and temperature. *J. Chem. Phys.* 2005, 123, 114714.
[83] Chen J, Zhang G, Li B. Substrate coupling suppresses size dependence of thermal conductivity in supported graphene. *Nanoscale* 2013, 5, 532–536.
[84] Guo Z, Zhang D, Gong XG. Thermal conductivity of graphene nanoribbons. *Appl. Phys. Lett.* 2009, 95, 163103.
[85] Nika DL, Askerov AS, Balandin AA. Anomalous size dependence of the thermal conductivity of graphene ribbons. *Nano Lett.* 2012, 12, 3238–3244.
[86] Cahangirov S, Topsakal M, Aktürk E, Şahin H, Ciraci S. Two- and one-dimensional honeycomb structures of silicon and germanium. *Phys. Rev. Lett.* 2009, 102, 236804.
[87] Jo I, Pettes MT, Kim J, Watanabe K, Taniguchi T, Yao Z, Shi L. Thermal conductivity and phonon transport in suspended few-layer hexagonal boron nitride. *Nano Lett.* 2013, 13, 550–554.
[88] Sahoo S, Gaur AP, Ahmadi M, Guinel MJF, Katiyar RS. Temperature-dependent Raman studies and thermal conductivity of few-layer MoS2. *J. Phys. Chem. C* 2013, 117, 9042–9047.
[89] Xie H, Hu M, Bao H. Thermal conductivity of silicene from first-principles. *Appl. Phys. Lett.* 2014, 104, 131906.
[90] Bo L, Reddy CD, Jinwu J, Hongwei Z, Julia AB, Sergey VD, Kun Z. Thermal conductivity of silicene nanosheets and the effect of isotopic doping. *J. Phys. D Appl. Phys.* 2014, 47, 165301.
[91] Zhang X, Xie H, Hu M, Bao H, Yue S, Qin G, Su G. Thermal conductivity of silicene calculated using an optimized Stillinger-Weber potential. *Phys. Rev. B* 2014, 89, 054310.
[92] Hu M, Zhang X, Poulikakos D. Anomalous thermal response of silicene to uniaxial stretching. *Phys. Rev. B* 2013, 87, 195417.
[93] Jing Y, Hu M, Guo L. Thermal conductivity of hybrid graphene/silicon heterostructures. *J. Appl. Phys.* 2013, 114, 153518.
[94] Kubota Y, Watanabe K, Tsuda O, Taniguchi T. Deep ultraviolet light-emitting hexagonal boron nitride synthesized at atmospheric pressure. *Science* 2007, 317, 932–934.
[95] Cai YQ, Lan JH, Zhang G, Zhang YW. Lattice vibrational modes and phonon thermal conductivity of monolayer MoS2. *Phys. Rev. B* 2014, 89, 035438.

[96] Thripuranthaka M, Kashid RV, Rout CS, Late DJ. Temperature dependent Raman spectroscopy of chemically derived few layer MoS2 and WS2 nanosheets. *Appl. Phys. Lett.* 2014, 104, 081911.
[97] Pop E, Varshney V, Roy AK. Thermal properties of graphene: fundamentals and applications. *MRS Bull.* 2012, 37, 1273–1281.
[98] Li XB, Maute K, Dunn ML, Yang RG. Strain effects on the thermal conductivity of nanostructures. *Phys. Rev. B* 2010, 81, 245318.
[99] Wei N, Xu LQ, Wang HQ, Zheng JC. Strain engineering of thermal conductivity in graphene sheets and nanoribbons: a demonstration of magic flexibility. *Nanotechnology* 2011, 22, 105705.
[100] Yang N, Ni XX, Jiang JW, Li BW. How does folding modulate thermal conductivity of graphene? *Appl. Phys. Lett.* 2012, 100, 093107.
[101] Cao AJ, Qu JM. Kapitza conductance of symmetric tilt grain boundaries in graphene. *J. Appl. Phys.* 2012, 111, 053529.
[102] Zhang HJ, Lee G, Cho K. Thermal transport in graphene and effects of vacancy defects. *Phys. Rev. B* 2011, 84, 115460.
[103] Haskins J, Kinaci A, Sevik C, Sevincli H, Cuniberti G, Cagin T. Control of thermal and electronic transport in defect-engineered graphene nanoribbons. *ACS Nano* 2011, 5, 3779–3787.
[104] Hao F, Fang DN, Xu ZP. Mechanical and thermal transport properties of graphene with defects. *Appl. Phys. Lett.* 2011, 99, 041901.
[105] Mortazavi B, Rajabpour A, Ahzi S, Remond Y, Allaei SMV. Nitrogen doping and curvature effects on thermal conductivity of graphene: a non-equilibrium molecular dynamics study. *Solid State Commun.* 2012, 152, 261–264.
[106] Zhang HJ, Lee G, Fonseca AF, Borders TL, Cho K. Isotope effect on the thermal conductivity of graphene. *J. Nanomater.* 2010, 2010, 537657-5.
[107] Konatham D, Striolo A. Thermal boundary resistance at the graphene-oil interface. *Appl. Phys. Lett.* 2009, 95, 163105.

Bionotes

Yanan Yue
School of Power and Mechanical Engineering, Wuhan University, Wuhan, Hubei 430072, China

Yanan Yue obtained his bachelor's and master's degrees in thermal engineering from Wuhan University, China, in 2007 and 2009, respectively. He obtained his PhD in Mechanical Engineering from Iowa State University in 2011. He joined DOE-Industrial Assessment Center at University of Wisconsin-Milwaukee working as the Manager and the Research Associate in Mechanical Engineering after a short Postdoc research experience at Iowa State University in 2012. In 2013, he joined the faculty of School of Power and Mechanical Engineering at Wuhan University, China. Currently, he is an Associate Professor and the Director of Micro/Nanoscale Thermal Characterization Lab at Wuhan University. His research interests focus on the thermal characterization and energy applications of nanostructured materials.

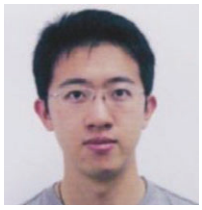

Jingchao Zhang
Holland Computing Center, University of Nebraska, Lincoln, NE 68588, USA

Jingchao Zhang received his bachelor's degree in thermal power engineering from Shandong University in 2010 and his PhD degree in Mechanical Engineering from Iowa State University in 2013. He is now an HPC applications specialist at the University of Nebraska Lincoln. His current research focuses on thermophysical property characterizations of micro/nanoscale materials like graphene, carbon-nanotube, and boron-nitride. Classic molecular dynamics (MD) simulations are performed in his studies on phonon thermal transport in micro and nano domains.

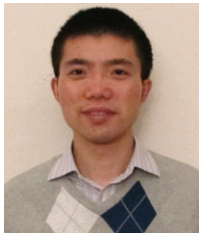

Xiaoduan Tang
Department of Engineering, Thrustmaster of Texas, Inc., Houston, TX 77065, USA

Xiaoduan Tang received his Bachelor's degree in Energy and Power Engineering in 2008, and his Master's degree in Thermal Engineering in 2010 from Xi'an Jiaotong University, China. In 2013, he obtained his PhD degree in Mechanical Engineering from Iowa State University, USA. Since January 2014, he has been working as an engineer in the Engineering Department of Thrustmaster of Texas, Inc. His research interests include thermal/mechanical characterization and structural analysis.

Shen Xu
Department of Mechanical Engineering, Iowa State University, Ames, IA 50010, USA

Shen Xu received her Bachelor's degree in Material Science from East China University of Science and Technology, China, in 2008 and her MS in Optics from Fudan University, China, in 2011. Currently, she is a PhD candidate in Micro/Nanoscale Thermal Science Laboratory, Department of Mechanical Engineering, Iowa State University. Her research interests include transient thermal probing technology development based on Raman thermometry and transient electrothermal technique, characterization of cross-plane thermophysical properties of thin films, 2D atomic-layer interface study, protein transformation study with thermal process, and heat transfer in near-field optics.

Xinwei Wang
Department of Mechanical Engineering, Iowa State University, Ames, IA 50010, USA,
xwang3@iastate.edu

Xinwei Wang received his BS (1994) and MS degrees (1996) from the Department of Thermal Science and Energy Engineering of University of Science and Technology of China. In 2001, he graduated with a PhD degree from the School of Mechanical Engineering of Purdue University. At present, he is a full professor with the Department of Mechanical Engineering of Iowa State University, and the director of Micro/Nanoscale Thermal Science Laboratory. The current research in his laboratory includes 2D atomic-layer interface energy transport, energy transport in proteins, and new nanoscale thermal probing to achieve atomic-level resolution. He is the inaugural recipient of the Viskanta Fellow of Purdue University in recognition of his independent and innovative research in the field of thermal sciences. He is an associate fellow of AIAA and fellow of ASME.

Graphical abstract

Yanan Yue, Jingchao Zhang, Xiaoduan Tang, Shen Xu and Xinwei Wang

Thermal transport across atomic-layer material interfaces

DOI 10.1515/ntrev-2014-0024
Nanotechnol Rev 2015; x(x): xxx–xxx

Review: The latest advances in experimental and theoretical studies of thermal transport across atomic-layer interfaces are presented, and the potential problems and opportunities are discussed.

Keywords: 2D atomic-layer; graphene; interface; Raman spectroscopy; thermal resistance.